The Thesis Committee for Paria Esmatloo
certifies that this is the approved version of the following thesis:

Fingertip Position and Force Control for Dexterous Manipulation through Accurate Modeling of Hand-Exoskeleton-Environment

APPROVED BY

SUPERVISING COMMITTEE:

Ashish D. Deshpande, Supervisor

James Sulzer

Fingertip Position and Force Control for Dexterous Manipulation through Accurate Modeling of Hand-Exoskeleton-Environment

by

Paria Esmatloo,

THESIS

Presented to the Faculty of the Graduate School of

The University of Texas at Austin

in Partial Fulfillment

of the Requirements

for the Degree of

MASTER OF SCIENCE IN ENGINEERING

THE UNIVERSITY OF TEXAS AT AUSTIN

May 2019

Acknowledgments

I would like to express my gratitude towards my advisor Dr. Deshpande for his help and support, for trusting me and believing in me even when I doubted myself, and for being patient with me as I grew in my graduate school experience. He has taught me to be an independent thinker and decision maker, to put myself in the shoes of my audience to see the subject from their perspective, and to always care about my peers and colleagues beyond my work responsibilities. I feel blessed to have worked with him and I look forward to our future collaborations.

I want to thank my dear husband, and my best friend Ramin Sabbagh, who has been by my side in every step of this journey. He has celebrated every little success with me and has been a great support and the best motivator whenever I struggled. I sincerely thank him for being my biggest fan and for his patience to survive through all my nagging and self-doubts. I could have not done this without him.

I am forever grateful to my parents who have always put my needs and prosperity before their own and have taken all measures to ensure I continue to grow to my full potential. My father has been the biggest role model for me growing up not only for his curiosity towards the world, but also for his patience and good manners. My mother has gone above and beyond in taking

care of me and my brother and providing all the means for a peaceful and nurturing environment for us. Together they have raised me to dream big and to believe sky is the limit. It is always heartwarming to feel their rock solid support throughout my life.

I would like to thank Dr. James Sulzer, for agreeing to be a reader on this thesis, and for his valuable feedback. I have learned and used important concepts from his "Intro to Robotics" course and I will never forget his humble and joyful attitude in the class.

I thank Dr. Youngmok Yun for his guidance and support especially in my first two years of the graduate school. He has introduces me to amazing life-changing research. He has helped me learn how to do research and how to improve people's life by it. His can-do attitude and his positive perspective towards life has been very inspiring. Dr. Youngmok Yun and Dr. Priyanshu Agarwal together have invented and built the Maestro exoskeleton, which has been a basis for my research. I am grateful for their contributions to rehabilitation robotics research and for their help and support whenever I go to them for help. Dr. Agarwal has provided many important insights which has helped me greatly in my thesis.

I would also thank my fellow members of the Reneu Robotics Lab, Dr. Taylor Niehues for being very responsive and helpful whenever I asked him confusing questions about thumb, Matthew Times, for his calming presence and great ideas to move the hand exoskeleton research forward, Dr. Prashant Rao for helping everyone around the lab, Ana Oliveira, for her warm support

and her humble and inspiring personality, Dr. Chad Rose, for proofreading my thesis and for the exemplary support he has provided to the lab in the past year, Job Remirez, for always helping us around with Mechanical Designs, Kaci Madden, Anna Shaffer, Alfredo Serrato, Rohit Varghese, Kevin Warburton, Patrick Marino, Keya Ghonasgi, and Mincheol Kim. One of the best parts of being a member of the ReNeu Lab is getting to share it with all of you. Thanks for making it an environment that I look forward to coming to everyday.

Fingertip Position and Force Control for Dexterous Manipulation through Accurate Modeling of Hand-Exoskeleton-Environment

Paria Esmatloo, M.S.E.
The University of Texas at Austin, 2019

Supervisor: Ashish D. Deshpande

Despite mechanical advancements in the design of hand exoskeleton devices to help people with hand disabilities regain partial hand function, their manipulation performance has remained far inferior compared to the human hand. State-of-the-art control strategies implemented on exoskeletons are mainly focused on robot joint-level position control, although accurate control of fingertip positions and forces is a requirement for reaching human-like dexterity and manipulation. The relationships between inputs (motor commands) and outputs (fingertip positions and forces) are highly nonlinear due to the inherent limitations in actuation structure of multiple degree of freedom (DOF) exoskeletons. Moreover, the simplified coupled models of finger joint movements do not hold when humans interact with external objects and exert forces at their fingertips. Therefore achieving dexterous manipulation will

require accurate models of interaction between the fingers, hand exoskeleton system, and fingertip environment.

In this thesis we accomplish, for the first time, fingertip position and force control with an assistive multi-DOF hand exoskeleton through accurate modeling of the hand-exoskeleton-environment. First, we provide kinematic and kinetic models for the human fingers, robot structure, and the Bowden cable power transmission for a fully actuated hand exoskeleton design. Next, we validate the models in simulation and demonstrate the successful control of fingertip position and forces in everyday drawing tasks. Finally, we utilize an experimental setup with a finger exoskeleton unit with two actuated DOF attached to an instrumented testbed finger to demonstrate successful tracking of fingertip position and forces within human accuracy levels through model-based control.

Table of Contents

List of Figures

Chapter 1

Introduction

Human dexterity and hand function are a result of combining various capabilities such as independent finger movement, reaction speed, strength, coordination, and precise control of task-specific fingertip forces [25]. Throughout the years, assistive devices have been developed to help people with hand disabilities regain partial independence in their daily activities. The assistive devices range from simple grippers and reachers such as $Featherlite^{TM}$ reachers, to one degree of freedom (DOF) exoskeletons such as IntelliArm [33], to complicated multi-DOF exoskeletons capable of actuating individual fingers [17, 43]. The earlier versions of assistive hand devices had focused on only one function in the fingers, such as pinching or opening and closing of the fingers [5, 13]. Recently, more advanced mechanisms have been developed to actuate the fingers in forms of exoskeletons or assistive gloves [15, 1, 2, 23]. Despite the development of many multi-DOF assistive exoskeletons, the quality of grasping, and the range of tasks that are performed by these devices, have been far inferior to that of the human hand.

Most of these advanced devices have only focused on whole hand movements and improving strength, disregarding many other prominent aspects of human dexterity such as independent finger movement, coordination, and precise control of fingertip forces. Despite the advancements in the exoskeleton design, most of the assistive research platforms used for grasping and manipulation have utilized the simplest forms of control strategies, such as robotic position control, for opening and closing the fingers [13], or coupled the movement of finger joints [31, 15]. Although these approaches can be effective in

improving some specific grasping needs, they ignore and even limit the various capabilities of humans in interacting with the objects in daily range of manipulation tasks, depriving them from achieving rich human-like manipulation. For instance, in [27] authors have used a finger exoskeleton to help Spinal Cord Injury (SCI) subjects with pinching tasks based on Electromyography (EMG) input from their muscles. The results showed that subjects were able to pinch some objects such as a rubber ball or a roll of tape. However, they were unable to grasp objects with different sizes and surface properties, e.g. a toothbrush or a deck of cards; which required different finger position and force configuration. In a more recent study, Yun et al. [43] implemented a pattern-recognition-based control to categorize the intent of SCI subjects into one of five grasp modes. The addition of various grasp modes combined with inherent compliance of the exoskeleton allowed subjects to grasp a variety of object shapes. However, subjects had difficulty completing the tasks that involved grasping small objects such as nuts and zippers, and also the tasks that required moving fingers in a precise manner such as doing up buttons, or folding a paper and putting it in an envelope. To achieve dexterous manipulation, assistive devices need to provide more than just an open-and-close mode, or even few grasping modes. When interacting with objects, humans require precise control of finger movements and fingertip forces depending on the task requirements.

Achieving accurate position and force control at the fingertips through an assistive device requires an accurate model of the complex system of human

hand, assistive device mechanisms and power transmission system, environment, and the interactions between them, besides an exoskeleton design that can actuate individual DOF of the fingers. There have been a few attempts to achieve models of the components of this system. The human hand is an important part of this system with a multifaceted structure. Many researchers have tried to model the human hand and fingers as mechanical structures with joints and linkages [28, 9]. Others have studied the constraints of joint and finger movements [26, 8]. Some of these constraints are due to anatomical structure of the hand. Other constraints describe the inter-finger and intra-finger relationships and couplings between joint movements, either in free motion, or in a few grasp categories. The latter has been proposed to reduce the number of DOF of the hand. Although these relationships can be helpful in describing the finger motions in achieving some gestures and specific conditions, these limitations generally do not hold when humans interact with external objects and apply forces at their fingertips [29]. Therefore, it is essential to use appropriate models of the human fingers that can fulfill the requirements of the manipulation task.

The second important component of the system is the assistive device or the exoskeleton. Many hand exoskeleton studies contain kinematic models of the devices that have been developed [37, 38, 15, 32, 24, 1, 41]. However, only a few of them have closely considered the interactions between the fingers and the exoskeleton and have tried to control the precise motion of the finger joints [42, 1, 37, 24]. In [24], authors have achieved a model of a finger exoskeleton

to perform exoskeleton joint position control and fingertip force control for virtual interaction in the direction of flexion. Whereas achieving human-like grasping and dexterous manipulation requires complete multi-finger models of the assistive devices, fingers, and the interactions between them to enable control of fingertip forces and positions within the functional workspace of the hand.

In this thesis, we aim to take an important step towards realizing human-like grasping and manipulation through assistive hand exoskeletons by accomplishing the following objectives: 1) We provide kinematic and kinetic models for human fingers, and finger-exoskeleton interaction for a fully actuated finger exoskeleton design, as well as a model for compensating slack (backlash) in the Bowden-cable transmission. 2) We validate the developed kinematic and kinetic models using simulation results for an everyday drawing task. 3) We demonstrate experimental results for fingertip position and force tracking through model-based control with a 2-DOF finger exoskeleton system and an instrumented finger within human finger accuracy.

The methodology presented in this thesis will pave the way for achieving human-like grasping and manipulation through assistive hand orthoses enabling accurate control of fingertip position and forces. More complex control strategies such as stiffness or impedance control, which has been shown to be effective in manipulation and human robot interaction [18], will be possible to implement once the kinematic mappings and the interaction models between the components of the system are available. Moreover, these findings

can potentially be translated to haptics and virtual reality applications where the specifics of the virtual environment and the task are well-known.

The rest of the thesis is structured as follows. In Chapter 2, we discuss previous research about hand exoskeleton design, human hand modeling, hand exoskeleton kinematic modeling, power transmission inaccuracies and control methodologies used for hand exoskeletons. In Chapter 3, we propose a fully actuated design for a finger exoskeleton. Then we present our developed model which considers the structure of human finger bones as well as linkage structure of a fully actuated exoskeleton and the power transmission system. We provide models for exploring the kinematic relationships between fully actuated finger exoskeleton and the human fingers. In Chapter 4, we validate the kinematic and kinetic models of the hand and exoskeleton and demonstrate simulation results for a finger exoskeleton with fully actuated degrees of freedom assisting the finger to achieve a sample task of drawing a circle with the fingertip while maintaining a constant interaction force. In Chapter 5, we present results by accurate tracking of finger movements, fingertip position, and fingertip forces using model-based control on a simpler robotic system comprised of an instrumented test-bed finger and a two degree of freedom index finger module of the Maestro hand exoskeleton [1, 43]. Next, we discuss the results, and make suggestions for further improving the control and modeling. Finally, the conclusion of the investigation work and future work are discussed in Chapter 6.

Chapter 2

Background

Assistive hand devices have been studied for the last few decades. Despite many efforts resulting in mechanical design advancements of these devices, their grasping and manipulation performance does not compare to human abilities. Going towards human-like grasping and manipulation through assistive devices requires accurate control of fingertip forces and positions. In this chapter we describe the requirements to make this goal possible, and review the background work in hand exoskeleton designs, power transmission systems, human hand and exoskeleton modeling and control to lay the groundwork for the methodologies presented in this thesis.

2.1 Hand Exoskeleton Designs

Assistive hand exoskeleton devices have been developed to help people with hand disabilities regain partial independence or recover from disabilities. Although the human hand is a very complex system with nearly 27 DOF, earlier devices such as [5, 13] focused only on coupled 1-DOF motion of the fingers, restraining fingers to only open and close in a pinching or cylindrical grasping motion. These devices can help with one specific grasp type when performing a well understood and defined task in a controlled environment. However, to achieve human-like grasping and manipulations, assistive systems need to provide more than a few types of grasping modes. Humans interact with a wide range of objects in daily tasks and fulfill the requirements of each task by accurately controlling the fingertip forces and positions. Later on, other devices were developed to actuate more DOF in the fingers to allow a wider

range of natural grasps [17, 43, 37, 24]. The small size of the finger phalanges and limited space in the hand make the design of a multi-DOF assistive hand exoskeleton a challenge. Unlike upper-body and lower body exoskeletons, it is often impossible to apply direct matching between the robot and finger joint motions due to limited space between the fingers. Moreover, direct matching requires knowledge about the exact linkage lengths and customization for each finger size [1]. Therefore many multi-DOF hand exoskeleton systems have used linkage mechanisms mounted on the back of the hand to actuate the finger joints [1, 24, 21, 38, 20]. In these mechanisms finger bones and joints are a part of the actuation mechanism. Although the mechanical linkage design provided a solution for the direct matching problem and multi-DOF actuation of joints, it makes the precise control of the finger movement challenging. The relationship between exoskeleton joint angle movements and the finger joint angle movements is usually nonlinear unless a parallelogram mechanism is implemented. In practice, the parallelogram mechanisms are not always ideal since the link lengths need to be adjusted according to exact individual finger link lengths [14], and misalignment might occur [24]. In general, when accurate control of finger joint motions, fingertip positions, or fingertip forces is of interest, an accurate kinematic or dynamic model of the hand-exoskeleton system is required. This system comprises of exoskeleton structure, power transmission mechanism and human hand. In the following sections, we will review the related work in the models developed in the literature for these subsystems and the control methods used to control the interactions between

the robotics exoskeleton system, fingers, and the environment.

2.2 Human Hand Modeling

The human hand is an important part of the system and has a very complex structure. Human hand is considered to have 27 DOF including six DOF for the wrist. Since the hand exoskeletons usually assist with the finger movements and leave the wrist free to move, we are mainly interested in finger structures and the ranges of motion. There has been attempts in the literature to model human fingers as mechanical linkages. In [28], authors have tried to achieve a linkage structure model of the human hand using optical motion capture data. They have proposed six DOF for CMC joint of the thumb, three DOF for proximal joints of each finger, and one DOF for other finger joints. In [34], authors have taken a closer look at the thumb linkage structure and have characterized the natural variability in linkage structure among individuals. In another work [9], authors have proposed what they call efficient kinematic models for manipulation tasks. They have simplified their 24-DOF realistic hand model with some motion constraints to a nine-DOF and a six-DOF model for circular and prismatic grasping. There are other studies which have considered the constraints in finger movements as well [8, 40]. Authors in [40] have tried to generate the natural hand postures utilizing motion constraints. On the other hand, [8] focuses on characterizing kinematic and dynamic constraints of the human hand. Other than anatomical constraints on the ranges of motion of each finger joint, authors have found relationships

coupling the movements of different joints of the same finger (intrafinger constraints), or coupling the movements of two joints in different fingers (inter finger constraints) in natural hand motion. Although these constraints can help with simplifying the hand models and reducing the total DOF of the model, they are mainly applicable only to free (unloaded) movement of the fingers. The coupling relationships are no longer accurate once the fingers are in contact with external objects and during grasping and manipulation tasks. For instance, although humans are not able to individually control the movement of the distal joint of the fingers in free movement, they are able to control this DOF when there is an external force on the fingertip during grasping and object manipulation. Therefore, it is necessary to use an appropriate model of the human hand for interaction with robotic exoskeletons and external objects. Such model should take into account the anatomical range limits of the joints, but should allow for the independent movement of the finger joints when necessary for manipulation tasks. In the modeling chapter, we will explain in detail the linkage structure model used in this research and the range of motion limitations imposed for human joints.

2.3 Hand Exoskeleton Modeling

Hand exoskeleton modeling has been considered in the literature mainly for the purpose of exoskeleton design and range of motion analysis, and rarely for real time control of precise movements of fingers or forces in object interactions. For instance, in [32, 15, 6] authors have developed kinematic models

of highly underactuated finger and thumb exoskeletons respectively, and have tried to optimize the design parameters such that the pe-defined 1DOF trajectory of the fingertip is close to that of the free human finger movement. Authors in [1, 37] have developed kinematic models for the exoskeleton and finger movements. However, they have only empirically validated position control at the exoskeleton joint level, and have not considered controlling and validating the finger joint angles or fingertip position. In [24], authors have achieved a kinematic model of the exoskeleton, as well as a dynamic model to compensate for robot hindrance in virtual reality applications. Similarly, position control validation has only been carried out in exoskeleton joint level.

2.4 Power Transmission Modeling

As mentioned before, for rehabilitation and assistive purposes, it is desired to keep the exoskeleton lightweight. Mounting the motors and actuators directly on the hand exoskeleton, although used in some exoskeleton designs [35, 36], is not ideal as it increases the weight and size of the device attached to the arm. To overcome this problem, other hand exoskeleton devices have implemented power transmission mechanisms such as cable driven actuation [7, 23, 39, 1], or flexible shaft transmission [37]. Among these, some are limited only to perform position control through the transmission system [7, 23, 39], and need to take into account power transmission losses or feedback from force sensors to control the interaction forces. Whereas some others [1, 3] who have implemented Series Elastic Actuation (SEA), or flex-

ible shafts [37] have the ability to control the transmitted torques through actuation. Although very limited research has been conducted on validating the accuracy of precision movements at the finger level, even the preliminary results on exoskeleton joint level position control show that losses in the power transmission system can significantly affect the position tracking results even in controlling the exoskeleton joint angles [24, 38, 37]. Therefore, compensating losses in the transmission system is an important step in achieving accurate position control and force control in hand exoskeletons. In [42], authors have characterized the backlash property in Bowden cable transmission system, and have proposed a model to perform feed forward torque control at the fingers by compensating for Bowden cable backlash. Considering the significance of transmission losses for accurate position control and force control applications, we will utilize a model for the transmission system inspired by [42], as well as kinematic and kinetic models for the exoskeleton and hand interactions.

2.5 Hand Exoskeleton Control Methods

Hand exoskeletons and soft wearable orthoses have been developed to provide therapy and rehabilitative exercises [37, 1, 20, 16, 4], assistance in daily tasks [43, 17, 31], virtual and haptics interactions [14, 22, 46], or a mixture of them [24, 23]. Human hands are capable of performing versatile grasping and manipulation tasks involving movements of various finger joints, and performing precise control of finger positions and interaction forces. Although the exoskeleton designs have become drastically more complex allowing for

multi-finger tasks and multi-joint actuation within fingers, aspiring to reach human finger mobility levels, the exoskeleton control strategies have remained mainly over-simplified and rudimentary compared to human hand abilities.

Many hand exoskeletons and assistive devices have focused on performing only one grasping mode, limiting the finger motion to a pre-defined trajectory, and considering whole-hand movements [27, 13, 19, 6]. It has been shown that although this assistance is beneficial in completing a limited range of grasping tasks, it can limit and even hinder the subject's ability to fulfill grasping and manipulation tasks involving objects with different shapes and sizes or requiring different force exertion patterns [13]. In fact, authors in [43] have reported that even with the addition of four grasping poses based on grasp taxonomy, pre-defined position control is not sufficient to satisfy the grasping and manipulation needs in activities of daily living (ADL). Subjects in this study were unable to perform tasks involving manipulation of small objects, exertion of low forces, and requiring versatile movement of fingers such as doing up buttons, folding a paper, or picking up nuts and bolts. This highlights the importance of precise control of position of fingers and interaction forces in successful completion of daily tasks.

A majority of the assistive hand literature has focused only on position control of devices, neglecting the importance of controlling interaction forces in object interactions and daily grasping and manipulation tasks [43, 44, 1, 6]. Most studies, despite using multi-DOF robots capable of actuating individual finger joints, have looked into validating the control of exoskeleton joint posi-

tions without considering precise control of finger movements [38, 24]. In [1] authors have provided a simulation scenario for controlling the finger joint angles through an index finger exoskeleton. Torque control at the finger joint level is performed in [42], and validated using an instrumented mechanical finger. Fingertip force for haptics applications has been studied by [14, 24], in which force tracking has been achieved for haptics applications. However, since the device used in [14] is focused on haptics applications, it does not have the ability to actuate different joints of the finger, and includes a heavy design on the back of the hand, and sensors on both sides of the fingertip to monitor and control the fingertip forces. Although the addition of the force sensors and the underactuated simple design helps in virtual applications, it is not a suitable design and control method for assistive applications and object interactions. Similarly, in [24], authors depend on a force sensor reading located at the fingertip to perform fingertip force control for virtual interactions. This limits the ability to perform object interactions and to apply forces in the extension direction of the fingers.

In the following chapters we demonstrate how we have addressed the issues of exoskeleton modeling and control to achieve precise tracking of finger movements, and fingertip positions and force through model-based control within human accuracy.

Chapter 3

Modeling

In this section we detail the modeling methodology used for kinematic modeling of human hand structure, hand-exoskeleton interactions, and Bowden cable actuation system. These models demonstrate the transformations between the motor inputs, exoskeleton joints, finger joints and fingertip space movements. Moreover, in the following chapters, they are used to track fingertip trajectories and forces through model-based control.

We have made a number of assumptions with the modeling work. It is assumed that the precision fingertip tasks are performed in low velocities. Moreover, the masses of fingers and exoskeleton are relatively small. Therefore quasi-static assumptions are considered and dynamic effect are neglected at this point. Finger joints are modeled as mechanical friction-less revolute joints with no parallel stiffness, with the attachments between the exoskeleton and fingers assumed to be rigid.

3.1 Human Finger Model

In this part we model the kinematics and kinetics of the human hand based on the bone structure of the human fingers. We introduce a hierarchical linkage structure of the index finger based on human anatomy similar to [9]. We also define the finger and joint constraints.

3.1.1 Linkage Structure

The linkage structure of human index finger is shown in Figure 3.1. There are four DOF in the the human index finger, namely, MCP abduction-

adduction (ab-ad), MCP flexion-extension (f-e), PIP flexion-extension (f-e), DIP flexion-extension (f-e). We have assumed the ab-ad axis and the f-e axis at the MCP joint of the finger are intersecting (universal joint), and perpendicular. The PIP and DIP f-e axes are perpendicular to the links (bones) attached to them. Note that the middle finger has the same linkage structure as the index finger.

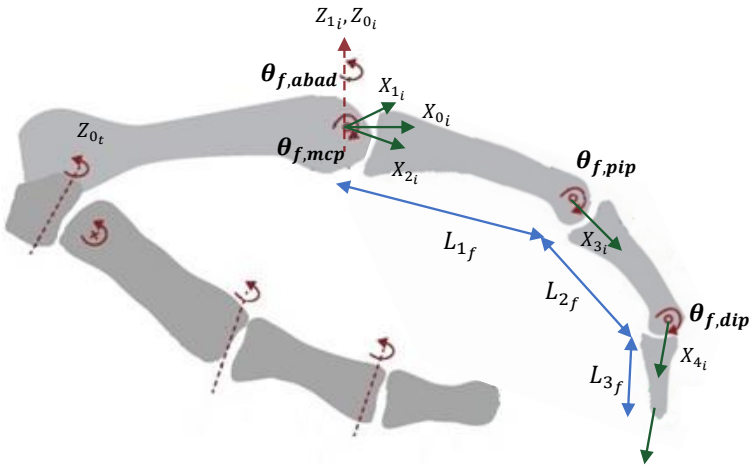

Figure 3.1: Linkage structure of human finger

3.1.2 Joint Limits

The joint motion limits of the human finger are chosen based on [12], and are listed in Table 3.1.

Joint	Minimum	Maximum
MCP	30° extension 35° abduction	90° flexion 35° adduction
PIP	0° extension	110° flexion
DIP	0° extension	70° flexion

Table 3.1: Human index (middle) finger joint limits

3.1.3 Kinematic Model

In this section we aim to achieve the kinematic model of the human index (and middle) finger motion. We assume rigid links and revolute joints, and utilize the modified Denavit-Hartenberg method [11] to describe the motion of the finger. The DH-parameter Table for the index (and middle) finger is shown in Table 3.2.

Joint	θ_i	α_{i-1}	a_{i-1}	d_i
1	$\theta_{f,abad}$	0	0	0
2	$\theta_{f,mcp}$	$\pi/2$	0	0
3	$\theta_{f,pip}$	0	L_{1_f}	0
4	$\theta_{f,dip}$	0	L_{2_f}	0
5	0	0	L_{3_f}	0

Table 3.2: DH parameters for human index finger

In this table, $\theta_{f,abad}$ is the abduction-adduction angle of the finger at the MCP joint, $\theta_{f,mcp}$ is the relative flexion angle at the MCP joint, $\theta_{f,pip}$ is the flexion angle at the PIP joint, $\theta_{f,dip}$ is the flexion angle at the DIP joint of the finger. L_{1_f} is the length of the proximal phalanx, L_{2_f} is the

length of the intermediate phalanx, and L_{3_f} is the length of the distal phalanx. Using transformation matrices, we calculate the orientation and position of the coordinate systems attached to all the links. Therefore, the position of the fingertip is found as a function of the joint angles.

$$\begin{bmatrix} X_{f_t} \\ Y_{f_t} \\ Z_{f_t} \end{bmatrix} = f(\theta_{f,abad}, \theta_{f,mcp}, \theta_{f,pip}, \theta_{f,dip}) \tag{3.1}$$

3.1.4 Kinetic Analysis

In the next step, we calculate the Jacobian for the index (and middle) finger by differentiating the endpoint coordinates with respect to the joint variables. This differentiation can be done symbolically.

$$J_{finger} = \begin{bmatrix} \frac{\partial X_{f_t}}{\partial \theta_{f,abad}} & \frac{\partial X_{f_t}}{\partial \theta_{f,mcp}} & \frac{\partial X_{f_t}}{\partial \theta_{f,pip}} & \frac{\partial X_{f_t}}{\partial \theta_{f,dip}} \\ \frac{\partial Y_{f_t}}{\partial \theta_{f,abad}} & \frac{\partial Y_{f_t}}{\partial \theta_{f,mcp}} & \frac{\partial Y_{f_t}}{\partial \theta_{f,pip}} & \frac{\partial Y_{f_t}}{\partial \theta_{f,dip}} \\ \frac{\partial Z_{f_t}}{\partial \theta_{f,abad}} & \frac{\partial Z_{f_t}}{\partial \theta_{f,mcp}} & \frac{\partial Z_{f_t}}{\partial \theta_{f,pip}} & \frac{\partial Z_{f_t}}{\partial \theta_{f,dip}} \end{bmatrix} \tag{3.2}$$

In the kinetic analysis, we are interested in calculating the fingertip force resulted by torques applied at the finger joints. It can be found according to Equation 3.4.

$$\begin{bmatrix} \tau_{f,abad} \\ \tau_{f,mcp} \\ \tau_{f,pip} \\ \tau_{f,dip} \end{bmatrix} = J_{finger}^{T} \begin{bmatrix} F_{f,x} \\ F_{f,y} \\ F_{f,z} \end{bmatrix} \tag{3.3}$$

$$\begin{bmatrix} F_{f,x} \\ F_{f,y} \\ F_{f,z} \end{bmatrix} = (J_{finger}^{T})^{+} \begin{bmatrix} \tau_{f,abad} \\ \tau_{f,mcp} \\ \tau_{f,pip} \\ \tau_{f,dip} \end{bmatrix} \tag{3.4}$$

where $(J_{finger}^{T})^{+}$ is the left pseudo inverse of J_{finger}^{T}.

3.1.5 Inverse Kinematics

In controlling assistive devices, we need to know the inverse kinematics of the fingers as well. For instance, it is desired to choose the appropriate finger joint angles to position the fingertip at a desired point in space. We have already calculated the fingertip position as functions of the four joint angles.

Since there are four joint angles in the index (and middle) finger and three coordinates (X, Y, Z) to control, this problem is redundant. That is, there are infinite combinations of joint angle values that enables the finger to achieve a desired position in space. Different strategies can be used to solve this redundancy problem such as coupling the joint angles, or minimum joint angle deviation from a defined value. However, since our ultimate goal is to perform dexterous manipulation, which involves accurate control of the fingertip position, orientation, force and the contact properties between the fingers and the object, we have chosen to control the total flexion angle of

the finger (the absolute flexion angle of the last phalanx), as a measure of the orientation of the fingertip in Cartesian space, and the position of the fingertip. A similar approach has been implemented in [29] for controlling the fingertip orientation and grasping force. Therefore, the inverse kinematics solution determines the four angles based on the fingertip position, and the desired total flexion angle of the finger, $\theta_{f,total}$. We find the joint angles by solving the system of four equations and four unknowns.

$$f(\theta_{f,abad}, \theta_{f,mcp}, \theta_{f,pip}, \theta_{f,dip}) = \begin{bmatrix} X_{t,desired} \\ Y_{t,desired} \\ Z_{t,desired} \end{bmatrix} \quad (3.5)$$

$$\theta_{f,mcp} + \theta_{f,pip} + \theta_{f,dip} = \theta_{f,total} \quad (3.6)$$

3.1.6 Torque Calculation

Similarly, we calculate the required torques at the finger joints to achieve a desired fingertip force from Equation 3.3.

3.2 Hand Exoskeleton and Finger Interaction Model

In this section, we develop an accurate model for the interactions between the exoskeleton and the fingers. In order to precisely control the movements of the fingers and the forces involved in grasping and dexterous manipulation, it is essential to determine the mappings between exoskeleton and finger joint angles, and joint torques.

The exoskeleton design implemented in the following models is inspired

by the design of Maestro Hand Exoskeleton [1, 3], Maestro hand exoskeleton has three finger modules for index finger, middle finger, and thumb. In the Maestro exoskeleton, only two joints are actuated in each of the index and finger modules (MCP and PIP flexion extension joints), and the abduction-adduction DOF and the DIP flexion extension are free to move. However, in order to do fine manipulation, it is important to fully control the configuration of the finger according to the requirements of the task. Therefore, in the model used in this chapter, we assume a general design in which all four DOF are actuated in the index and middle fingers.

3.2.1 Index Finger-Exoskeleton Interaction Model

In this part we introduce the proposed design for the index (and middle) finger exoskeleton. Then we solve the forward and inverse kinematics for the mapping between the finger and the exoskeleton. We also derive the kinetic relationships and find the mapping between the torques at exoskeleton and finger joints.

3.2.1.1 Linkage Structure

The actuation of the four joints of the finger is done through three closed loop chains (Figure 3.2). The first chain of the exoskeleton is a slider-crank mechanism to actuate flexion-extension and abduction-adduction at the MCP joint. As discussed before, we have assumed that in index (and middle) finger, the flexion-extension and abduction-adduction joints are co-located. However,

in the exoskeleton, the first joint is the flexion-extension joint, and the second one is the abduction-adduction DOF. The slider on the proximal phalanx ensures that the forces transmitted between the exoskeleton and finger at that point are in the normal direction only. The kinematic solution for movement of this chain is presented in the next subsection.

After finding the kinematic solution for the first chain, the second chain of the exoskeleton and finger interaction can be simplified to a planar four-bar mechanism. In this mechanism, the exoskeleton MCP joint angle controls the finger MCP joint angle. The last chain of the exoskeleton is similar to the MCP chain and controls DIP flexion angle of the finger through a planar four-bar mechanism.

3.2.1.2 Kinematic Model

Starting from the first chain of the index-exoskeleton system, we want to find the finger MCP flexion-extension and abduction-adduction angles as functions of the input exoskeleton angles at the MCP joint. We assume abduction-adduction and flexion-extension joint axes at the finger MCP joint are intersecting and perpendicular, and the points A and B are grounded from hand and exoskeleton side respectively. We also assume that the points A, B, C, and D are always co-planar. At each abduction-adduction angle of the exoskeleton, the mechanism ABCD can be thought as an inverted planar crank-slider mechanism. Closed loop kinematics solution of this mechanism can be found in [30], which describes the flexion angle of the finger and the slider length l_{AD}

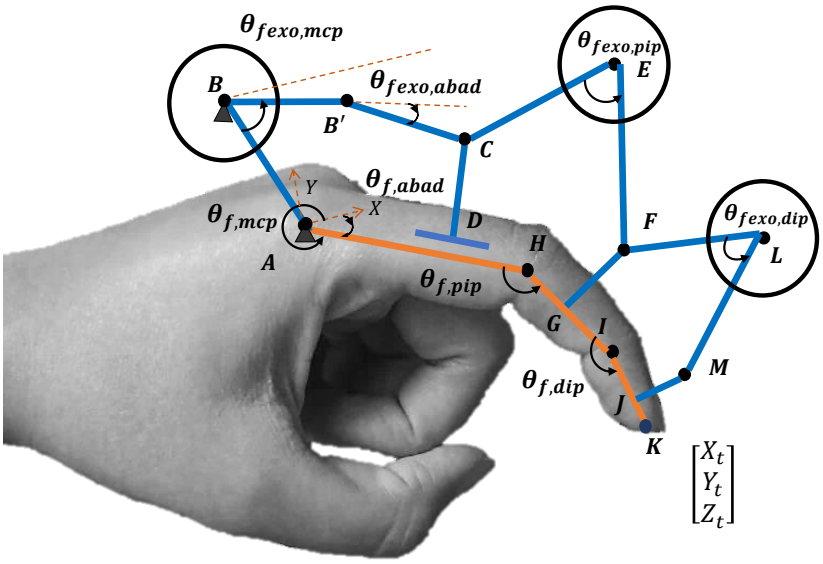

Figure 3.2: Index exoskeleton mechanism

in terms of exoskeleton angles and link lengths. Please note that the equivalent length l_{BC} can be found as a function of exoskeleton abduction-adduction angle according to the law of cosines (Equation 3.7).

$$l_{BC} = (l_{BB'}^2 + l_{B'C}^2 - l_{BB'} l_{B'C} cos(\pi - \theta_{fexo,abad}))^{1/2} \tag{3.7}$$

The closed form solution of the inverted crank slider mechanism gives two equations for $\theta_{f,mcp}$ and l_{AD}, which are also coupled with the third unknown $\theta_{f,abad}$.

We also have an additional equation for abduction adduction angles of

exoskeleton and the finger based on the co-planarity condition of the ABCD mechanism shown in Equation (3.8), which enforces the out-of-plane movement of points C and D to be equal. This gives us three equations and three unknowns, and by solving it we find the finger MCP angles based on exoskeleton angles.

$$\theta_{f,abad} = arcsin[l_{B'C} sin(\theta_{fexo,abad}) cos(\theta_{fexo,mcp,abs})/(l_{AD} cos(\theta_{f,mcp}))] \quad (3.8)$$

Next, for solving the second chain of the finger-exoskeleton interaction, we can consider the mechanism CEFH as a planar four-bar mechanism, with exoskeleton relative PIP angle as the input. Link lengths l_{CH} and l_{FH} can be calculated knowing the slider length calculated from inverted slider crank equations and other exoskeleton and finger link lengths. Using the solution for kinematics of the four-bar mechanism [30], finger PIP angle, $\theta_{f,pip}$, is calculated as a function of the exoskeleton PIP angle $\theta_{fexo,pip}$.

The last chain, or the DIP chain similarly utilizes a four-bar mechanism to actuate the DIP joint of the finger. The kinematics can be solved based on the four-bar equations, and the finger DIP angle, $\theta_{f,dip}$, is calculated as a function of the exoskeleton DIP angle, $\theta_{fexo,dip}$.

Finally, all the unknown finger joint angles are found as functions of the exoskeleton input angles (Equation 3.9).

$$\begin{bmatrix} \theta_{f,abad} \\ \theta_{f,mcp} \\ \theta_{f,pip} \\ \theta_{f,dip} \end{bmatrix} = f_{fexo}(\begin{bmatrix} \theta_{fexo,abad} \\ \theta_{fexo,mcp} \\ \theta_{fexo,pip} \\ \theta_{fexo,dip} \end{bmatrix}) \tag{3.9}$$

3.2.1.3 Kinetic Relationships

To find the kinetic relationships between exoskeleton joint torques and finger joint torques, we need to find the Jacobian. The Jacobian of the finger-exoskeleton system can be found by partial differentiation of finger joint angles with respect to exoskeleton joint angles (Equation 3.10). This differentiation can be carried out using symbolic operations in MATLAB and the `Jacobian` function.

$$J_{fexo} = \begin{bmatrix} \frac{\partial \theta_{f,abad}}{\partial \theta_{fexo,abad}} & \frac{\partial \theta_{f,abad}}{\partial \theta_{fexo,mcp}} & \frac{\partial \theta_{f,abad}}{\partial \theta_{fexo,pip}} & \frac{\partial \theta_{f,abad}}{\partial \theta_{fexo,dip}} \\ \frac{\partial \theta_{f,mcp}}{\partial \theta_{fexo,abad}} & \frac{\partial \theta_{f,mcp}}{\partial \theta_{fexo,mcp}} & \frac{\partial \theta_{f,mcp}}{\partial \theta_{fexo,pip}} & \frac{\partial \theta_{f,mcp}}{\partial \theta_{fexo,dip}} \\ \frac{\partial \theta_{f,pip}}{\partial \theta_{fexo,abad}} & \frac{\partial \theta_{f,pip}}{\partial \theta_{fexo,mcp}} & \frac{\partial \theta_{f,pip}}{\partial \theta_{fexo,pip}} & \frac{\partial \theta_{f,pip}}{\partial \theta_{fexo,dip}} \\ \frac{\partial \theta_{f,dip}}{\partial \theta_{fexo,abad}} & \frac{\partial \theta_{f,dip}}{\partial \theta_{fexo,mcp}} & \frac{\partial \theta_{f,dip}}{\partial \theta_{fexo,pip}} & \frac{\partial \theta_{f,dip}}{\partial \theta_{fexo,dip}} \end{bmatrix} \tag{3.10}$$

Having the Jacobian helps us calculate the resulting torques at the human joints as a result of the applied torques at the exoskeleton (Equation 3.12).

$$\begin{bmatrix} \tau_{fexo,abad} \\ \tau_{fexo,mcp} \\ \tau_{fexo,pip} \\ \tau_{fexo,dip} \end{bmatrix} = J_{fexo}^{T} \begin{bmatrix} \tau_{f,abad} \\ \tau_{f,mcp} \\ \tau_{f,pip} \\ \tau_{f,dip} \end{bmatrix} \tag{3.11}$$

$$\begin{bmatrix} \tau_{f,abad} \\ \tau_{f,mcp} \\ \tau_{f,pip} \\ \tau_{f,dip} \end{bmatrix} = (J_{fexo}^{T})^{-1} \begin{bmatrix} \tau_{fexo,abad} \\ \tau_{fexo,mcp} \\ \tau_{fexo,pip} \\ \tau_{fexo,dip} \end{bmatrix} \tag{3.12}$$

where $(J_{fexo}^{T})^{-1}$ is the inverse of J_{fexo}^{T}.

3.2.1.4 Inverse Kinematics

In this section we solve the inverse kinematic problem of the finger-exoskeleton interaction. This helps determine what angles should be chosen at exoskeleton joints to achieve a desired set of finger joint angles.

For this purpose, we go back to the mechanisms discussed previously (Figure 3.2). The finger MCP ab-ad and flexion angles are the inputs for the first chain. A similar co-planarity condition to Equation 3.8 is required at each abduction adduction angle. The mechanism ABCD can be thought of as a four-bar crank sider mechanism this time, and the solutions to unknown angles and the slider length can be found by solving the loop equations as shown in [30].

Inverse kinematic solution for PIP and DIP chains are found from solving the four-bar loop equations for the two loops. In these inverse problems, the inputs are the finger PIP and DIP angles and the outputs are the exoskeleton relative angles at PIP and DIP joints.

3.2.1.5 Torque Calculation

Torques required at the exoskeleton joints to achieve a desired set of torques at fingertips can be found from Equation 3.11.

3.3 Series Elastic Actuation Model

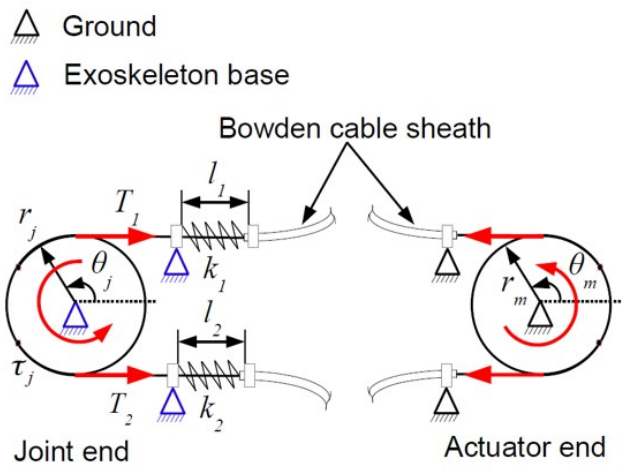

Figure 3.3: Series Elastic Actuation (SEA) used in exoskeleton design [1]

The Series Elastic Actuation (SEA) design is shown in Figure 3.3. One pulley is attached to the motor side, and another pulley is attached to the exoskeleton joint. There are two linear springs on both sides of the pulley on exoskeleton joint side to transmit torques. The power is transmitted through Bowden cables connecting the two pulleys, allowing remote positioning of actuators with respect to the hand exoskeleton. Assuming no loss in the Bowden cable mechanism, the exoskeleton joint torque relationship can be found based

on the displacement of the pulleys attached to the motor and exoskeleton joint, as well as the stiffness parameters of the SEA (Equation 3.13).

$$\tau_j = (T_2 - T_1)r_j = 2k(r_m\theta_m - r_j(\theta_j - \theta_{j0}))r_j \tag{3.13}$$

where τ_j is the torque at exoskeleton joint, T_1 and T_2 are the amount of tension forces in the cables, r_j is the joint pulley radius, r_m is the motor pulley radius, $(\theta_j - \theta_{j0})$ is the angular displacement of the exoskeleton joint with respect to resting angle.

If we assume that the effects of friction, exoskeleton inertia, and dynamic effects are negligible, and the transmitted torque is zero in steady state, the displacement of the Bowden cable on both sides would be equal. Based on these assumptions, the relationship between the angle displacements at exoskeleton and joints would be as shown in the Equation 3.14.

$$\theta_m = \frac{r_j}{r_m}(\theta_{j,d} - \theta_{j0}) \tag{3.14}$$

where $\theta_{j,d}$ is the desired exoskeleton joint angle.

3.3.1 Bowden Cable Slack Model

Bowden cables are used to transmit bidirectional torques by relative displacement of the inner cable and outer sheath. However, their position and torque transmission accuracy is dependent on pre-tension in the cable and bending in cable routing. In practice, Bowden cables demonstrate a behavior similar to fatigue due to Bowden cable slack (Figure 3.4), and do not

follow the relationship given in Equation 3.14 exactly. In [42], authors propose a mathematical model to express Bowden cable slack (backlash) behavior (Equation 3.15).

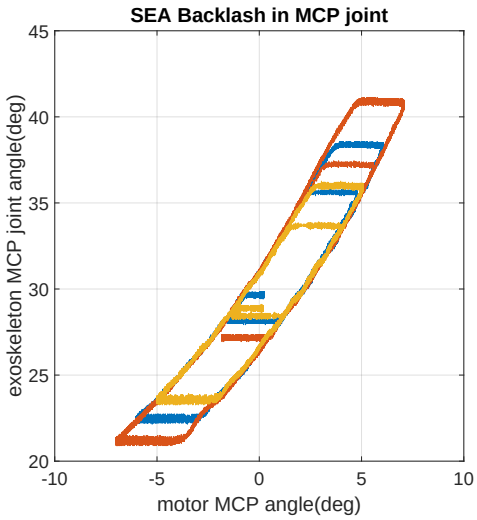

Figure 3.4: Bowden cable backlash effect shown in MCP joint of Maestro finger exoskeleton

$$\theta_j(t) = BL(\theta_m(t)) = \tag{3.15}$$
$$\begin{cases} \alpha(\theta_m(t) - c_r), & if\ \dot{\theta}_m(t) > 0 \quad \& \quad \theta_j(t^-) = \alpha(\theta_m(t^-) - c_r) \\ \alpha(\theta_m(t) - c_l), & if\ \dot{\theta}_m(t) < 0 \quad \& \quad \theta_j(t^-) = \alpha(\theta_m(t^-) - c_l) \end{cases}$$

where $\alpha = r_m/r_j$ and c_r, and c_l are the right and left offsets of the backlash curve, and should be obtained empirically.

In order to compensate for this backlash effect during exoskeleton motion control, authors propose a smooth backlash inverse model shown in Equation 3.16, which gives the motor position commands necessary to achieve a

desired exoskeleton angle.

$$\begin{aligned} \theta_{m,d}(t) &= SBL^{-1}(\theta_{j,d}(t)) = \theta_{j,d}/\alpha + c_r\gamma + c_l(1-\gamma) \\ \gamma(\dot{\theta}_{j,d}(t)) &= \frac{1}{1+exp(-\rho\dot{\theta}_{j,d}(t))} \end{aligned} \tag{3.16}$$

where γ is a sigmoid function and ρ is a positive constant determining the degree of smoothness. The larger the ρ, the sharper the changes in the commanded motor angles to compensate for the slack. We utilize the backlash inverse model to achieve accurate control of exoskeleton joint angle positions in the experimental validation chapter.

Chapter 4

Simulation

In this chapter, we validate the developed kinematic and kinetic models by simulating everyday scenarios. First we consider position tracking scenarios for following desired fingertip trajectories which include inverse and forward kinematics throughout the system. Next, we look at fingertip force tracking in which the magnitude and the direction of the force at the fingertip is controlled by inverse and forward kinematics and kinetic calculations through exoskeleton and finger joint torques.

4.1 Position Tracking

Accurate control of 3D fingertip position has not been commonly considered in hand exoskeleton literature. Previously, only feed-forward position control of the exoskeleton joints has been explored in which the exoskeleton joints are moved and the fingers follow a vague trajectory determined by the exoskeleton and finger interactions [1, 43, 10, 45]. Consequently, power grasping tasks with imprecise movements of fingers have been looked at as opposed to precision grasps and object manipulation which require fine movement of fingers and control of position and forces at the fingertips. However, having an accurate model of the system, we will be able to accurately control the 3D position of the fingers by choosing appropriate exoskeleton joint angles. Simulation results are shown in the following subsections for select trajectory tracking tasks.

In this section, we present the simulation results for a trajectory tracking task of following a circle with the index (or middle) fingertip. In this

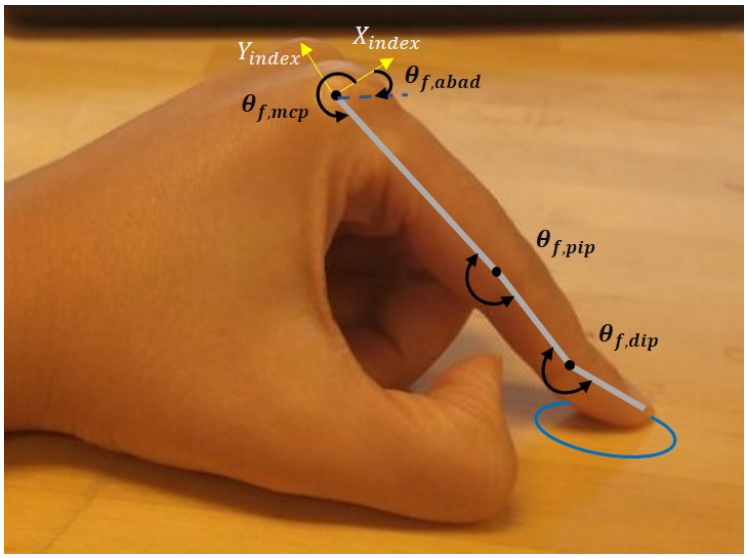

Figure 4.1: Configuration of the index finger while working with a touch screen

simulation, we consider the task of following a circle with a diameter of 1.4 cm on a touchscreen such as a tablet as shown in Figure 4.1. Based on real-world examples, we estimated the plane of the screen to make a 45° angle with the XZ plane of the index finger. In addition we chose to track the perimeter of a circle with a diameter of 1.4 mm on the touchscreen (Figure 4.2). First, the trajectory of the index fingertip is calculated to follow the perimeter of the circle at 12 data points. The X-Y-Z components of this trajectory in the inertial frame attached to the index finger metacarpal bone are plotted in Figure 4.3 in solid lines as the desired trajectories of the fingertip.

Next, joint angles are calculated using the inverse kinematic functions for following the desired 3D position of fingertip according to Equation 3.5. As discussed in the previous chapter, the index finger mechanism is redundant.

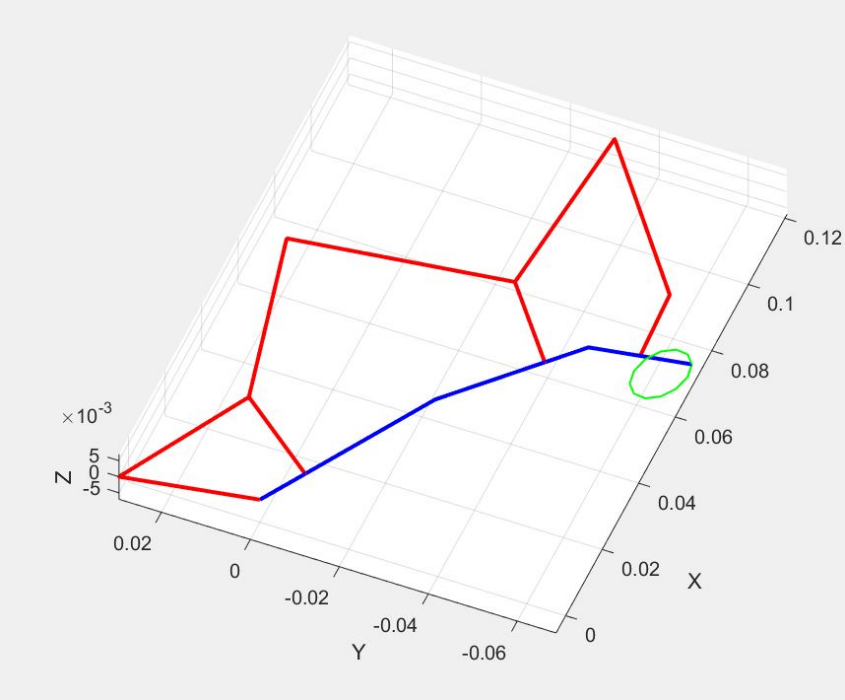

Figure 4.2: Circle trajectory tracking using the index fingertip

Thus, we can choose to control the desired flexion angle of the last phalanx of the finger (Equation 3.6) as well as the 3D position of the fingertip. In this simulation we chose the flexion angle of the distal phalanx of the index finger to be constant throughout the task. When an exact solution is not possible, we defined a cost function containing the errors in the 3D position of the fingertip and in the orientation of the last phalanx, as shown in Equation 4.1.

$$Cost_f = w_{x_f}\Delta X_{t_f}^2 + w_{y_f}\Delta Y_{t_f}^2 + w_{z_f}\Delta Z_{t_f}^2 + w_{\phi_f}\Delta\phi_f^2 \tag{4.1}$$

where ΔX_{t_f}, ΔY_{t_f}, and ΔZ_{t_f} are the errors in X coordinate, Y coordinate, Z coordinate of the fingertip position, and $\Delta\phi_f$ is the error in the flexion angle of

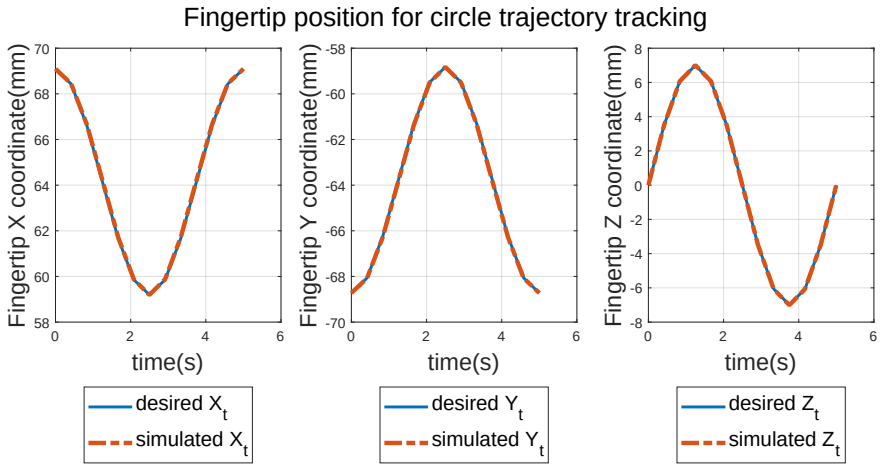

Figure 4.3: Desired (solid) and simulated position of the fingertip for tracking a circle trajectory

the distal phalanx. w_{x_f}, w_{y_f}, w_{z_f}, and w_{ϕ_f} are the corresponding weight values. The weight values can be altered based on the importance of the accuracies in a specific task. For instance, if we care more about the accuracy in following the circle trajectory at the fingertip, and less about the orientation of the distal phalanx, we can choose the weights on the X-Y-Z errors to be higher. The required finger joint angles calculated using the described method are shown in Figure 4.4 in solid lines. In the next step, the exoskeleton angles required to achieve these finger joint angles were found using the inverse kinematics of finger-exoskeleton interaction (Figure 4.5).

At this point, we have the inputs (exoskeleton joint angles) to the system to achieve the desired fingertip trajectory. To validate the accuracy of the complete model developed, we feed these values to the forward kinematics

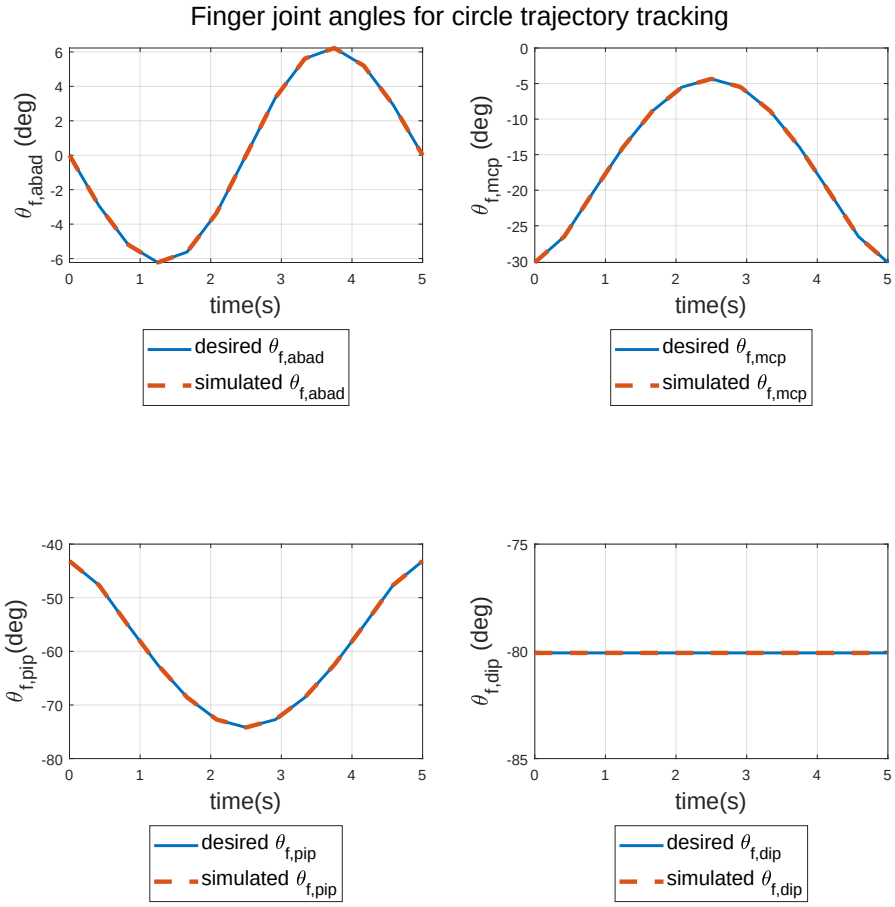

Figure 4.4: Finger joint angles for circle trajectory tracking task, as calculated from inverse kinematics (solid) and forward kinematics simulation

models for finger-exoskeleton interaction and human finger model. The resulting index finger angles are shown in Figure 4.4 in dotted lines. The solid lines and the dotted lines overlap which shows the accuracy of the model for achieving the desired trajectory. Next, we feed the achieved finger joint angles

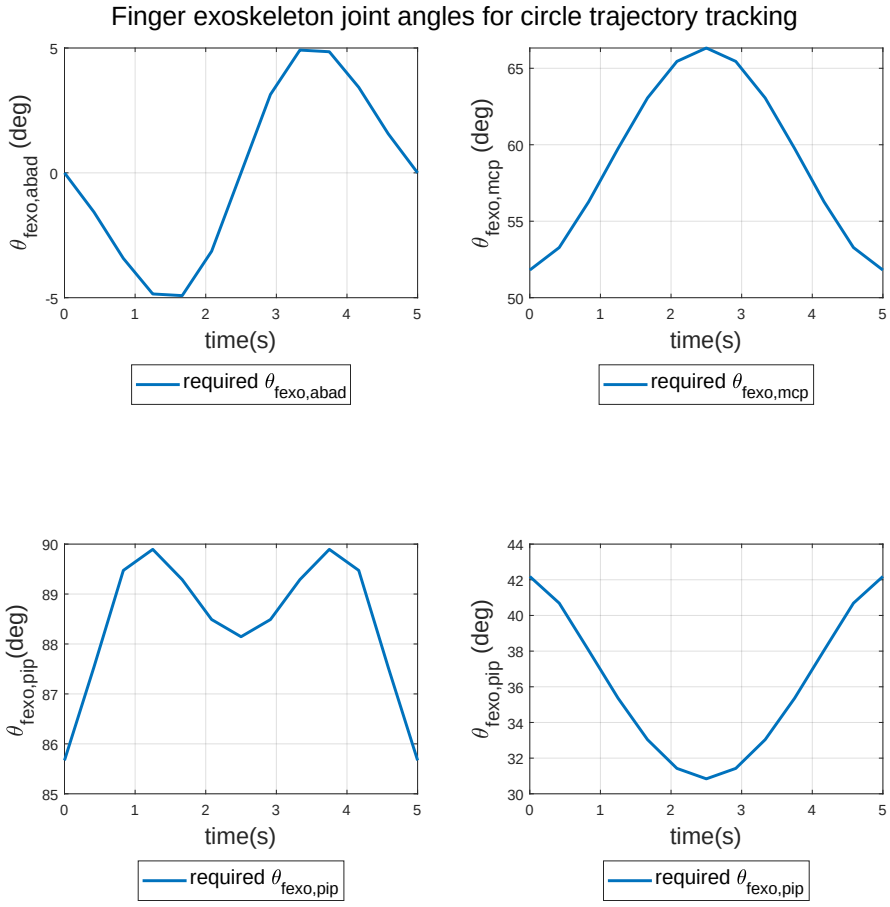

Figure 4.5: Index exoskeleton joint angles for circle trajectory tracking task, as calculated from inverse kinematics

to the human hand model and calculate the resulting fingertip trajectory in 3D. The results are shown in Figure 4.3 in dotted lines. Similar to finger joint angles, the simulated fingertip trajectory follows the desired trajectory as well, validating the accuracy of the model developed.

4.2 Fingertip Force Tracking

In this section, we validate the kinetic relationships developed for index exoskeleton system. Here, the objective for the fingertip is to maintain a constant force towards the plane of the circle (touchscreen) while following the circle trajectory. In this simulation, we set the desired fingertip force to be 0.5 N in a direction normal to the plane of the touchscreen at any point on the circle trajectory, which makes a 45° angle with the X-Z plane of the index finger (Figure 4.2).

Next, we can use the kinematic relationship derived for the human finger (Equation 3.3) to calculate torques required at the exoskeleton joints at each point to yield the desired fingertip force. The finger torques calculated based on this method to maintain the fingertip force while drawing the circle are shown in Figure 4.6 in solid lines. The kinetic relationships derived in the last chapter for finger-exoskeleton system (Equation 3.11) can be used to calculate required torques at exoskeleton joints to provide the desired fingertip force as shown in Figure 4.7. Once the exoskeleton joint torques are available, we feed it back to the forward kinematics models to find the resulting torques at finger joints (shown in dotted lines in Figure 4.6) and the simulated force at the fingertip (Figure 4.8).

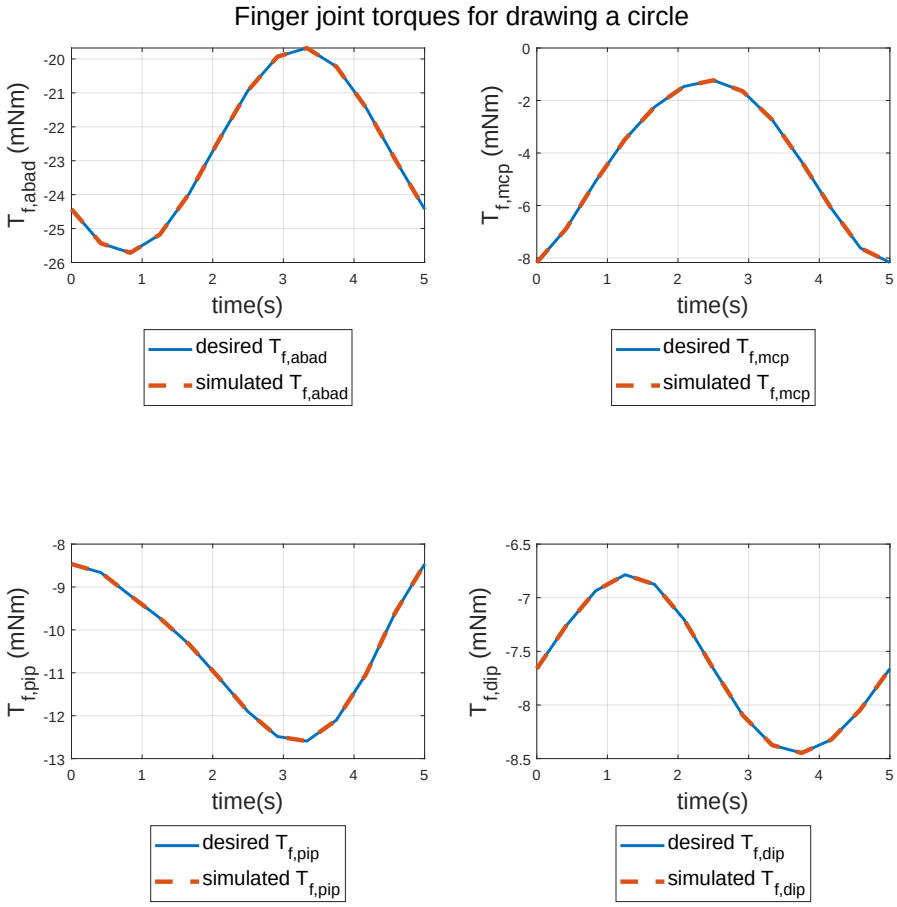

Figure 4.6: Desired and simulated torques at finger joints for drawing a circle on a touchscreen

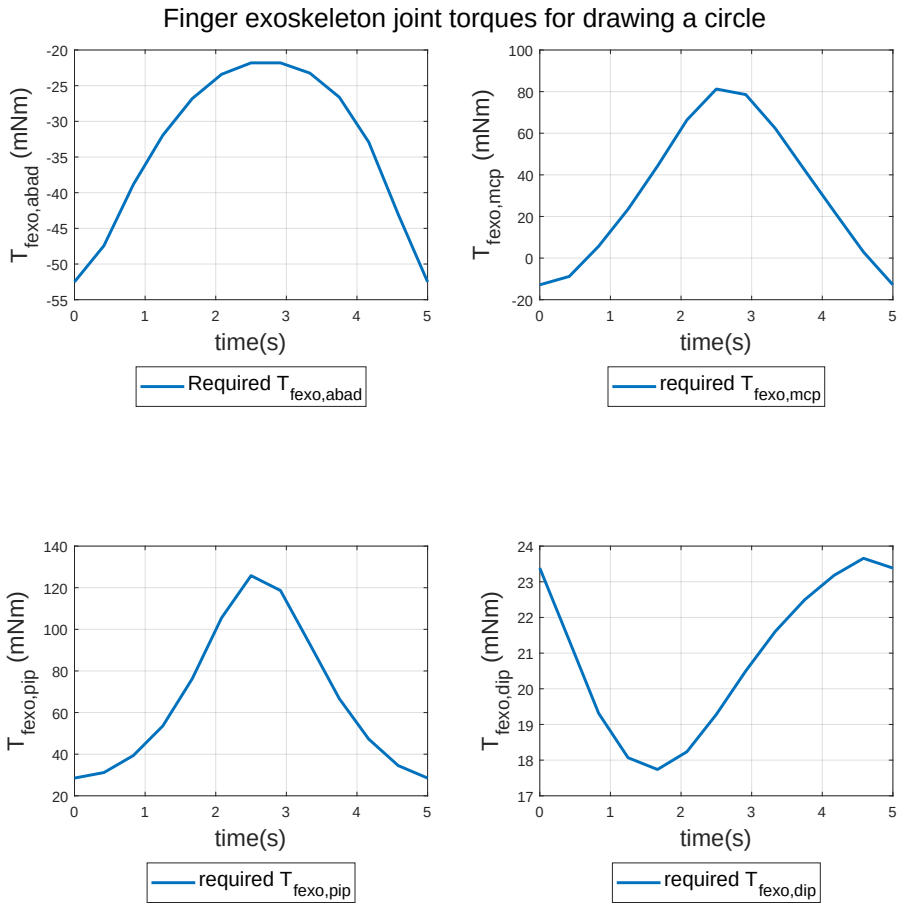

Figure 4.7: Required torques at finger exoskeleton joints for drawing a circle on a touchscreen

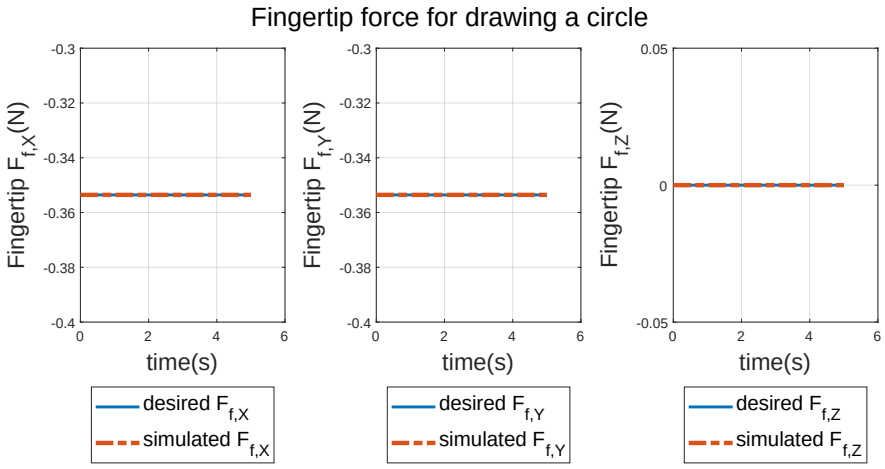

Figure 4.8: Resulting 3D force at the fingertip while drawing a circle on a touchscreen

It is apparent that in all the figures the simulated joint and torque trajectories (dotted lines) closely follow the desire values (solid lines) which validates the kinematics and the kinetic models developed for the finger-exoskeleton system. Note that we have neglected the effects of friction, and finger and exoskeleton inertia as well as the dynamic effects at this point. However, having the current model, we are able to perform various tasks requiring simultaneous control of fingertip positions and forces. In the future, we plan to improve the kinematic and kinetic models by adding the inertial effects, and passive joint properties.

Chapter 5

Experimental Characterization

5.1 Motivation

Precise control of finger movements and fingertip forces is essential for dexterous manipulation and fulfillment of daily tasks. To help users accomplish these tasks, exoskeletons should be able to provide the ability to perform fingertip position and force control. We proposed in the previous chapters that a model-based control considering the structure and interactions between fingers, exoskeleton, and environment, would enable this goal. In this chapter we utilize a 2-DOF finger exoskeleton module and an instrumented finger to implement the models that have been developed in the previous chapters in control of exoskeleton and finger movements and forces. We test the model-based control methods on an exoskeleton to compare the results with simulations, considering the real-world limitations, such as sensor value inaccuracies, error in link lengths in the model, friction and etc. We validate the position and force tracking results in exoskeleton joint, finger joint, and fingertip space levels. Moreover, we demonstrate a comparison case for a finger joint angle control case without using the kinematic models.

5.2 Methods

We utilize the index finger module of the Maestro exoskeleton [1, 43], with two actuated degrees of freedom to validate the kinematic and kinetic modeling developed in the previous chapters. To isolate the effects of different uncertainties in the system such as relative movement between finger and exoskeleton attachments and difficulty to measure exact finger joint angles,

we perform these preliminary experiments with an instrumented testbed finger instead of the human finger. The motivation for using the testbed finger is to have access to the accurate finger joint angles measured using sensors, and to minimize the effects of soft tissue and the movement of the attachments on the skin. We perform trajectory tracking in exoskeleton, finger and fingertip spaces, as well as force tracking experiments. The detailed experiment setup and methods used are explained in the following sections.

5.2.1 Experiment Setup

As shown in Figure 5.3, the experiment setup for the position tracking experiments consists of the index finger module of the Maestro exoskeleton, an instrumented finger with two joints mounted on a stand, and motion capture markers. On the other hand, the experiment setup for fingertip force tracking experiment also includes and a six axis force sensor grounded on a mechanical breadboard. The interface between finger and the force sensor includes compression springs to transmit forces in X and Y directions.

5.2.1.1 Exoskeleton Overview

Maestro hand exoskeleton [43, 1, 2] consists of three finger modules for index finger, middle finger, and thumb shown in Figure 5.1. In the original design, there are two actuated DOF in the index and middle fingers for actuating MCP joint flexion-extension, and PIP flexion-extension. The DIP flexion-extension, and the MCP abduction-adduction degrees of freedom are

free to move but not actuated in the original design [1]. The thumb module has four actuated DOF for the four joints. We will focus our attention on the index module, since the measurements of human joint angles for model validation are more accessible.

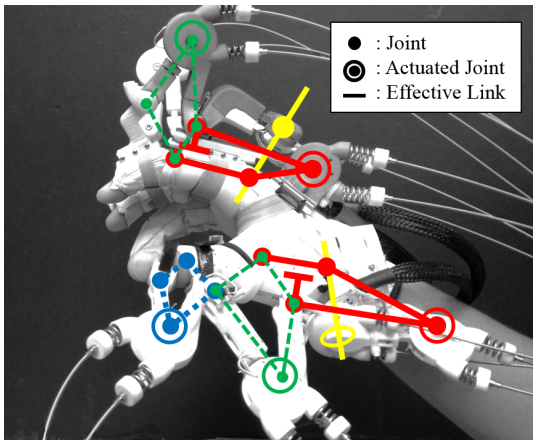

Figure 5.1: Maestro exoskeleton has three actuated fingers and 8 DOF. The actuation of the joints are done through slider-crank and four-bar mechanisms [43].

In the index exoskeleton, the actuation mechanisms are planar slider-crank mechanism in the first chain of the finger for actuating the MCP joint, and planar four-bar mechanism in the second chain for actuating the PIP joint. The abduction-adduction DOF at the MCP joint is allowed to move freely, and the abduction-adduction angle of the exoskeleton is measured by a sensor. The flexion-extension DOF of the DIP joint is linked to the exoskeleton DIP joint, which is equipped with joint angle sensors, through a planar four-bar mechanism for estimating the DIP joint angle of the finger. The actuation system in the Maestro exoskeleton is series elastic actuation, with pulleys and

springs at each actuated joint of the exoskeleton, enabling torque control at the exoskeleton joints.

In these experiments, we chose to work with the index module of the Maestro exoskeleton, with two degrees of freedom. Since we plan to perform Cartesian trajectory and force tracking at the fingertip, we only use the MCP and PIP joints, as they are the two joints that are actuated in the exoskeleton. We limited the movement at the MCP abduction-adduction through testbed finger design.

5.2.1.2 Instrumented Finger

Validation of the kinematic models that have been developed, namely the finger model and the finger-exoskeleton interaction model, requires accurate angle measurements in the finger joints. We use an instrumented finger, similar to the one used in a study by Yun et al. [42], to closely monitor the finger joint angles closely (Figure 5.2). In addition, using the instrumented finger with rigid attachments, we aim to minimize the unpredictable errors of skin movement, and attachment sliding. The instrumented finger is equipped with magneto-resistive sensors at joints which can be calibrated to accurately measure the joint angles. The exoskeleton is attached to the instrumented finger rigidly by the help of screws, slider attachment, and revolute joint. In our experiments, we take measurements of the joint angles, but we do not consider the passive stiffness of finger joints. We also use the dummy finger sensor values to 1) validate trajectory tracking results for finger joint angle

tracking and 2) use as feedback for control of finger joint movements without using the kinematic models as a comparison case.

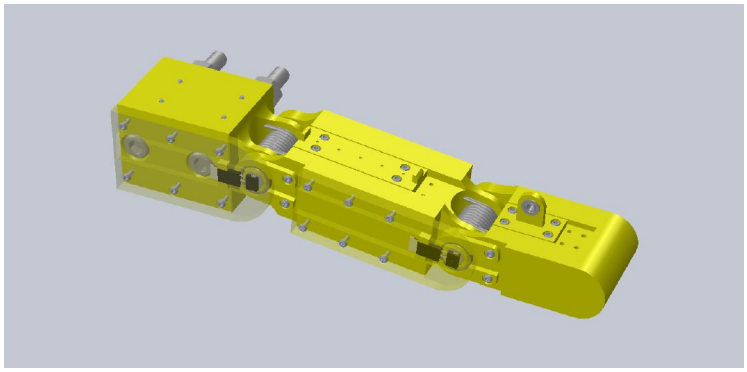

Figure 5.2: 3D CAD model of the instrumented testbed finger for validation of the kinematic model of interaction between the exoskeleton and fingers [42]

5.2.1.3 Force Sensing

Robotic fingers and exoskeletons should be able to accurately control the forces at the fingertips to perform fine grasping and manipulation tasks similar to human hands. To measure and validate the forces transmitted between the fingertip and the environment, we have used a six axis Robotous force/torque sensor (RFT40-SA01) shown in Figure 5.3.

5.2.2 Experiment Protocols

In the following sections we will explain the protocol for each of the experiments.

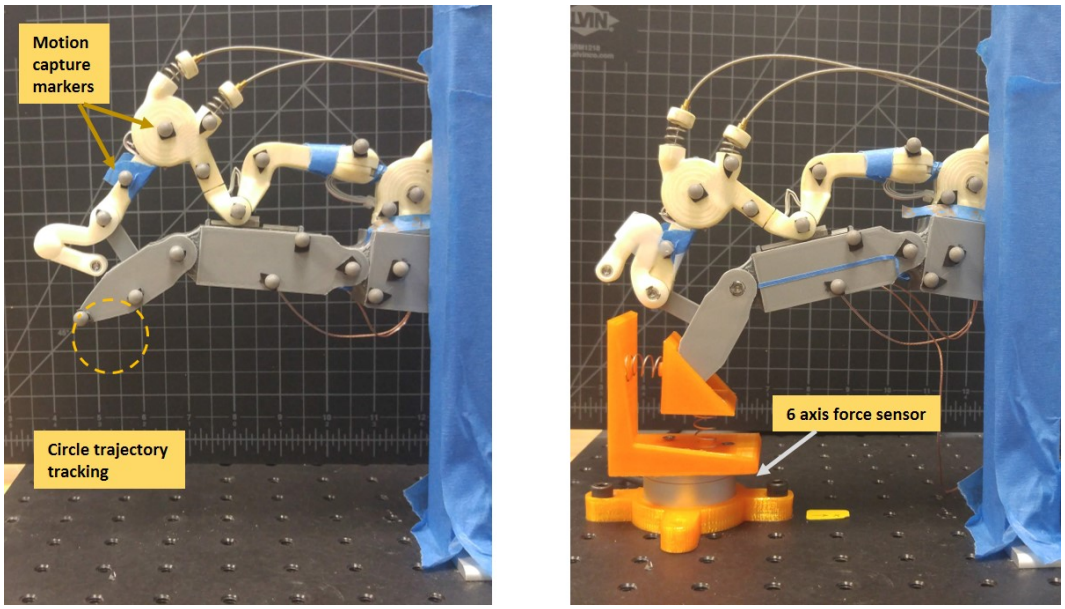

Figure 5.3: Experiment setup for trajectory tracking (left) and fingertip force tracking experiments (right)

5.2.2.1 Exoskeleton Joint Angle Tracking

In the first experiment, we validate accurate control of the exoskeleton joint angles. Accurate control of the exoskeleton joint angles, which are the inputs to kinematic models, is the first step in achieving accurate results at the finger and Cartesian levels. However, as mentioned in the modeling part, the slack in Bowden cable power transmission system results in inaccuracies in exoskeleton joint angle tracking. We examine the exoskeleton joint angle accuracy and compare the results for the two cases of 1) feedback control and 2) feedback control + backlash compensation.

The desired exoskeleton joint angles for MCP and PIP joints of the

exoskeleton are chosen to change as sinusoidal functions that oscillate about initial angles $\theta_{exo,mcp,0}$ and $\theta_{exo,pip,0}$, with amplitudes $\theta_{exo,mcp,A}$, and $\theta_{exo,pip,A}$

In the first experiment, we implement a feedback control method. However, in this case we assume the tranasmission losses and inaccuracies to be negligible. We implement a Proportional Integral (PI) controller to control the joint angle at the exoskeleton joints with the exoskeleton joint angle sensor as feedback to the controller (Equation 5.1).

$$\theta_m = \frac{r_j}{r_m}(\theta_{j,d} - \theta_{j0}) + K_P\theta_{j,error} + K_I \int \theta_{j,error} dt \tag{5.1}$$

where $\theta_{j,error} = (\theta_j - \theta_{j,d})$ is the error in exoskeleton joint angle tracking, K_P is the proportional gain and K_I is the integral gain.

In the second experiment we implement the backlash inverse model to compensate for Bowden cable slack in the transmission system. Instead of the feedforward term, we substitute the smooth backlash inverse term as introduced in the modeling section (Equation 5.3). The results of the two methods and the effects of using the backlash inverse model are discussed in the results section.

$$\theta_m = \theta_{j,d}/\alpha + c_r\gamma + c_l(1-\gamma) + K_P\theta_{j,error} + K_I \int \theta_{j,error} dt \tag{5.2}$$
$$\gamma(\dot{\theta}_{j,d}(t)) = \frac{1}{1 + exp(-\rho\dot{\theta}_{j,d}(t))}$$

5.2.2.2 Finger Joint Angle Tracking

In the next experiment, we determine the desired finger joint angle trajectories for the MCP joint and the PIP joint of the instrumented finger. The desired MCP and PIP joint angles follow a sinusoidal trajectory oscillating about initial angles $\theta_{f,mcp,0}$ and $\theta_{f,pip,0}$, with amplitudes $\theta_{f,mcp,A}$, and $\theta_{f,pip,A}$

We compared two different control methods for performing finger joint angle tracking. First, we utilized a simple feedback control method (Figure 5.4), assuming linear proportional relationships between exoskeleton and finger joint angles. Note that in practice, the relationships between the exoskeleton and finger joint angles are nonlinear and are described through kinematic models discussed in the modeling section. However, to create a comparison scenario for non-model based control, we assumed an estimated linear relationship (simple proportional model) between exoskeleton and finger joint angles (Equation 5.4) as a reference to compare with model-based control results. Please note that although this simple feedback method is chosen as an alternative to kinematic model-based control, the finger joint angle data is not readily available in human subject applications.

$$\delta\theta_{exo,mcp} \approx \delta\theta_{f,mcp} \tag{5.3}$$
$$\delta\theta_{exo,pip} \approx -\delta\theta_{f,pip}$$

In the second experiment, we implemented the kinematic model-based control taking into account the exoskeleton and finger interactions, as well as

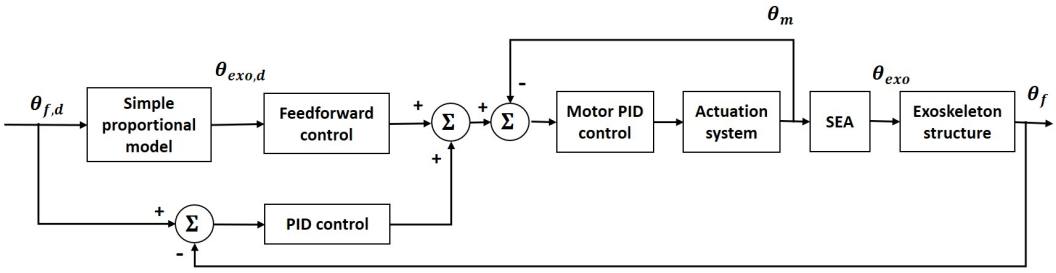

Figure 5.4: Finger joint angle control through simple feedback control using finger joint angle as feedback

the inverse backlash model to compensate for Bowden cable slack (Figure 5.5). The required exoskeleton angles are found based on inverse kinematic model of interaction, and controlled based on PI controller using exoskeleton joint angle sensor data as feedback. Note that this control method does not require finger joint angle data, which are difficult to monitor during human-robot interaction.

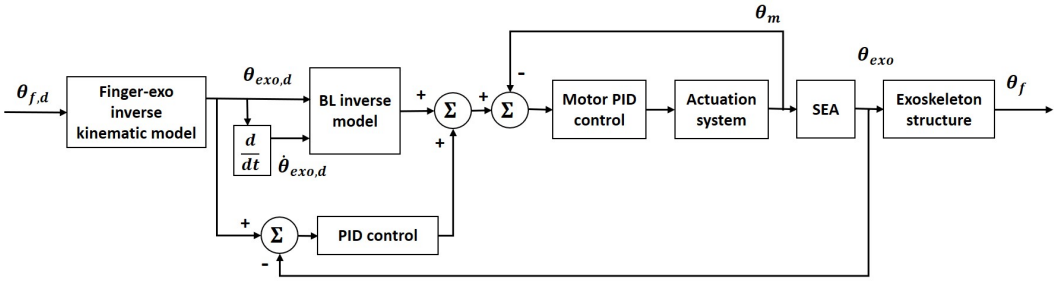

Figure 5.5: Finger joint angle model-based control utilizing kinematic models and Bowden cable backlash model

The results of the two controllers are discussed and compared in the results section.

5.2.2.3 Fingertip Position Tracking

In this experiment we command a desired fingertip Cartesian trajectory in X and Y directions. First, we chose X and Y trajectories of the fingertip to follow a vertical line with a height of 1.5 cm using the fingertip. In the next experiment, we chose X and Y trajectories to follow a circle trajectory in the plane of the finger using the fingertip. The circle diameter was chosen to be 1.5 cm. The frequency of the movement is 0.2 Hz. The control scheme is similar

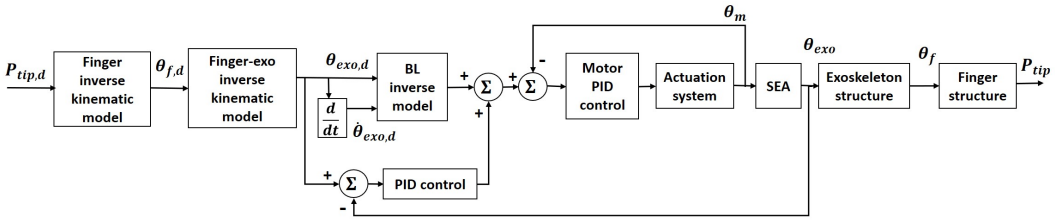

Figure 5.6: Fingertip position control utilizing kinematic models and Bowden cable backlash model

to model-based finger joint angle tracking. But it includes the finger inverse kinematics as well. The most proximal feedback source used in this control, similar to last experiment, is the exoskeleton joint angle sensor data. First, the finger inverse kinematics relationships are used to calculate the finger joint angles required to achieve the desired fingertip trajectory. Then the inverse kinematics relationships in exoskeleton-finger interaction give the required exoskeleton joint angles. Finally, the PI controller is used again to drive the exoskeleton.

The results are validated based on the motion capture data attained from markers attached to finger linkages and the fingertip as shown in Figure

5.3. The motion capture system used in this study is the OptiTrack system, and the gray spheres shown in the figure are passive markers attached to rigid bodies to find position and orientation of the bodies of interest. The reflective surfaces of the exoskeleton, and the attachments are covered with non-reflective materials (blue tape) to increase the accuracy of the motion capture experiment.

5.2.2.4 Human Finger Position Tracking

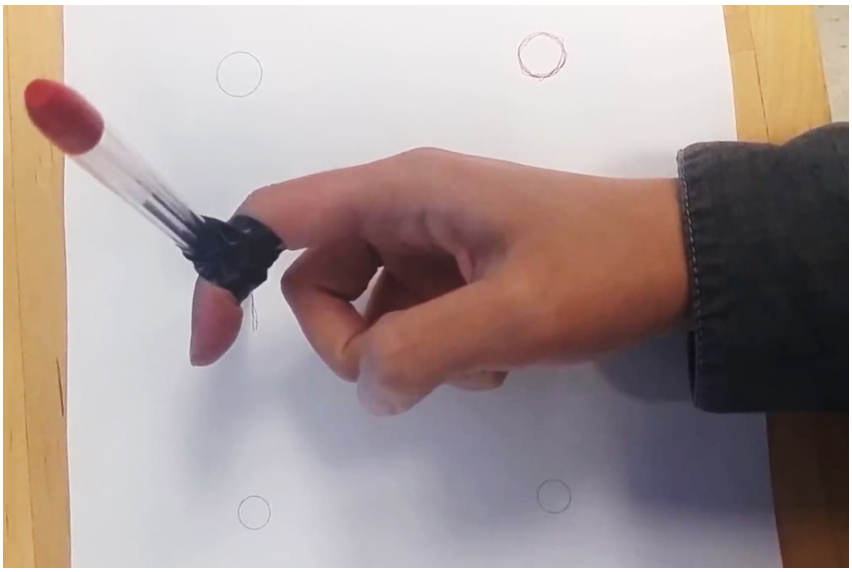

Figure 5.7: Trajectory tracking task with human finger. The pen is attached at the distal end of second phalanx to replicate the instrumented finger experiment.

In order to fairly evaluate position tracking accuracy of the implemented control, we asked a healthy subject to perform similar trajectory tracking tasks using their finger (Figure 5.7). A pen was fixed to the end of the

second phalanx of the finger (to be consistent with robot experiments), and an outline was prepared at a comfortable distance to allow trajectory tracking in a plane parallel to the plane of finger. The subject was asked to trace the vertical line and the circle trajectory in a periodic motion at their comfortable speed. Subject had access to the visual feedback from the experiment sheet.

5.2.2.5 Kinematic Model Performance Evaluation

We collect motion capture data from robot and testbed finger in order to evaluate the performance of kinematic models. Data is collected during a finger joint angle tracking task. We test the forward and inverse kinematic models by feeding the models ground truth position and angle data recorded by the motion capture system, and comparing the estimated outputs with recorded values from motion capture recordings.

5.2.2.6 Fingertip Force Tracking

In this experiment, we validate force tracking in Cartesian space at the fingertip. For this purpose we determine desired fingertip forces as sinusoidal trajectories. We place the force sensor and the attachment close to the fingertip so that the finger is tangentially in contact with the surface of the force sensor attachment. The experiment setup is shown in Figure 5.3. We choose the desired force trajectory as sinusoidal trajectories with components in horizontal and vertical directions. The controller utilizes kinematic and kinetic models to calculate the configuration-dependent Jacobian of the finger and the

finger-exoskeleton interaction (Figure 5.8). Once the desired torques (Equation 3.11) at the exoskeleton joints are calculated, a feedback torque controller is used to control the torque at the SEA.

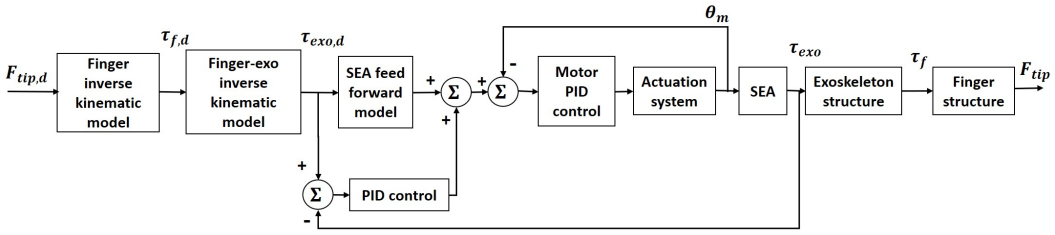

Figure 5.8: Fingertip force control utilizing kinematic models and feedback terms from exoskeleton SEA

5.3 Results

First, we take a look at motor position tracking performance, since this performance is the basis for all other control schemes. In Figure 5.9 the PIP motor tracking performance is shown as an example in different amplitudes and frequencies and percentage RMSE values are demonstrated for each case.

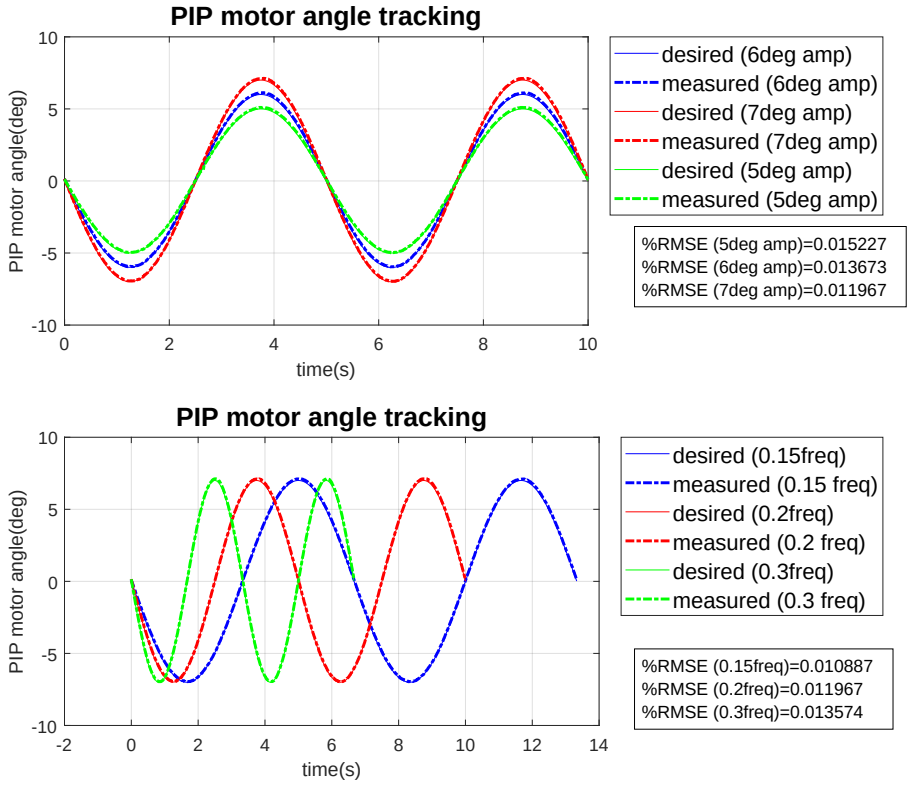

Figure 5.9: Motor angle tracking performance at three frequencies (0.15 Hz, 0.2 Hz, 0.3 Hz) and three amplitudes (5°, 6°, 7°)

In Figures 5.10 and 5.11 the exoskeleton angle tracking results are

shown for MCP and PIP joints respectively, when the PI controller is used based on feedback from exoskeleton angle sensors.

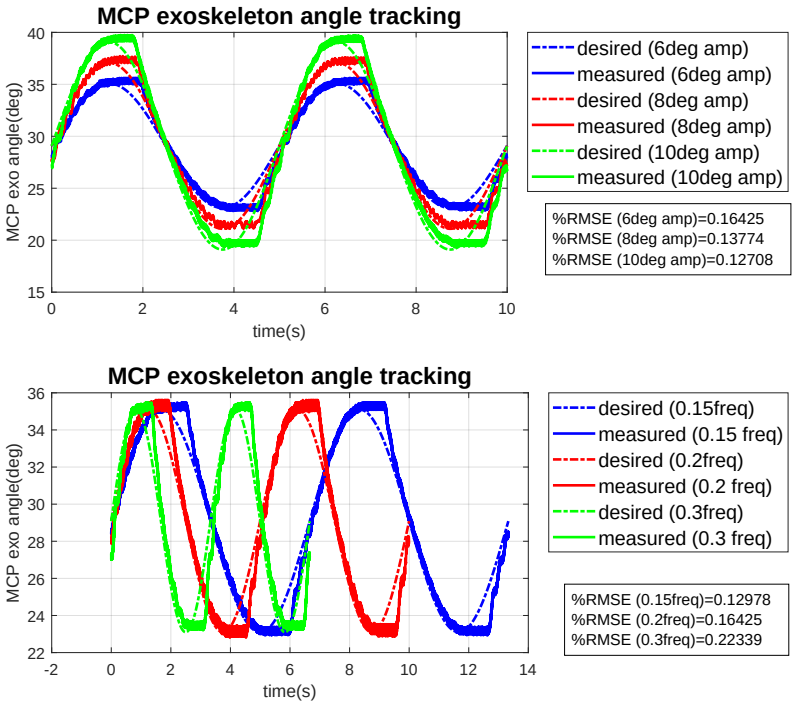

Figure 5.10: Exoskeleton MCP joint angle tracking using a PI controller at three frequencies (0.15 Hz, 0.2 Hz, 0.3 Hz) and three amplitudes (6°, 8°, 10°)

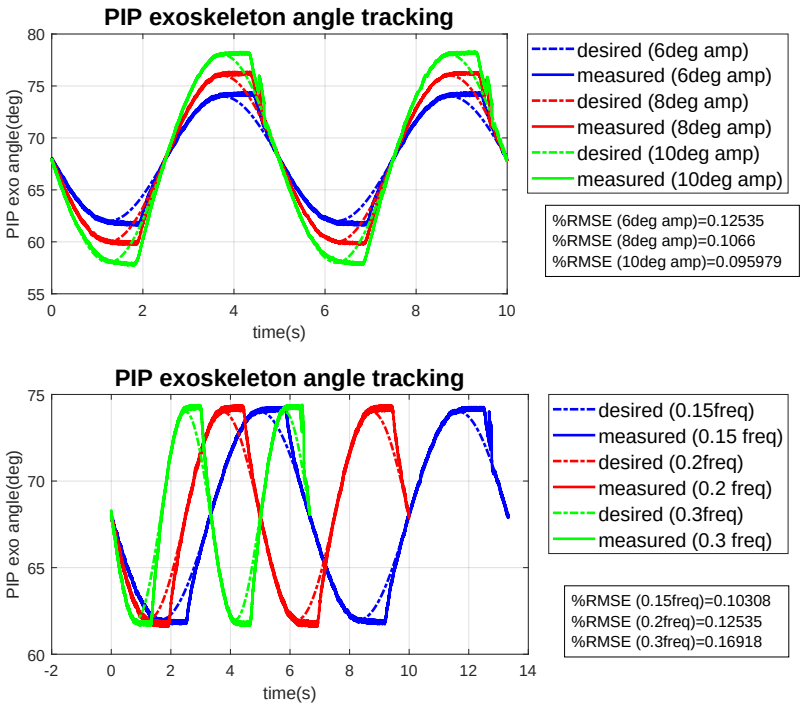

Figure 5.11: Exoskeleton PIP joint angle tracking using a PI controller shown at three frequencies (0.15 Hz, 0.2 Hz, 0.3 Hz) and three amplitudes (6°, 8°, 10°)

Figure 5.12 shows the results form simultaneous tracking of MCP and PIP joint angles using the feedback method.

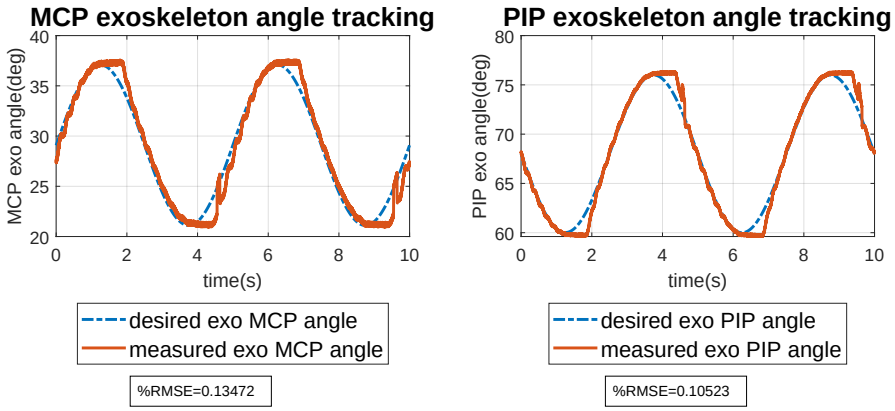

Figure 5.12: Simultaneous exoskeleton angle tracking at the MCP and PIP joints using a PI controller. Out-of-phase sinusoidal trajectories are tracked with a frequency of 0.2 Hz and amplitude of 8°.

Next, the effects of utilizing the Bowden cable backlash inverse model on exoskeleton joint angle tracking is demonstrated in Figures 5.13, and 5.14. The results are shown in different amplitudes and frequencies for comparison.

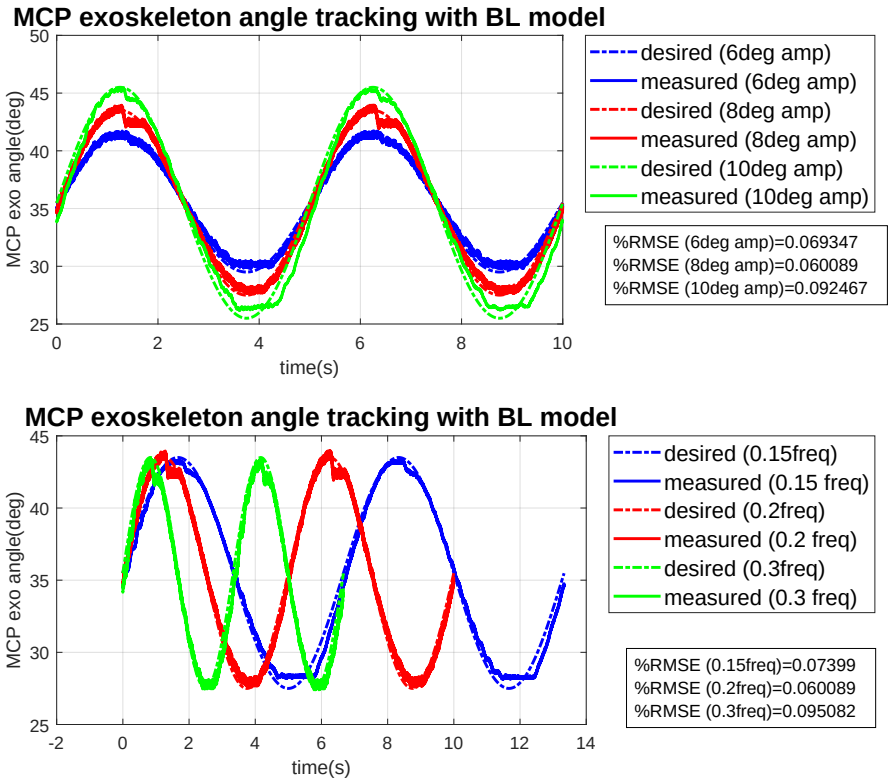

Figure 5.13: Exoskeleton MCP joint angle tracking using the backlash inverse model at three frequencies (0.15 Hz, 0.2 Hz, 0.3 Hz) and three amplitudes (6°, 8°, 10°)

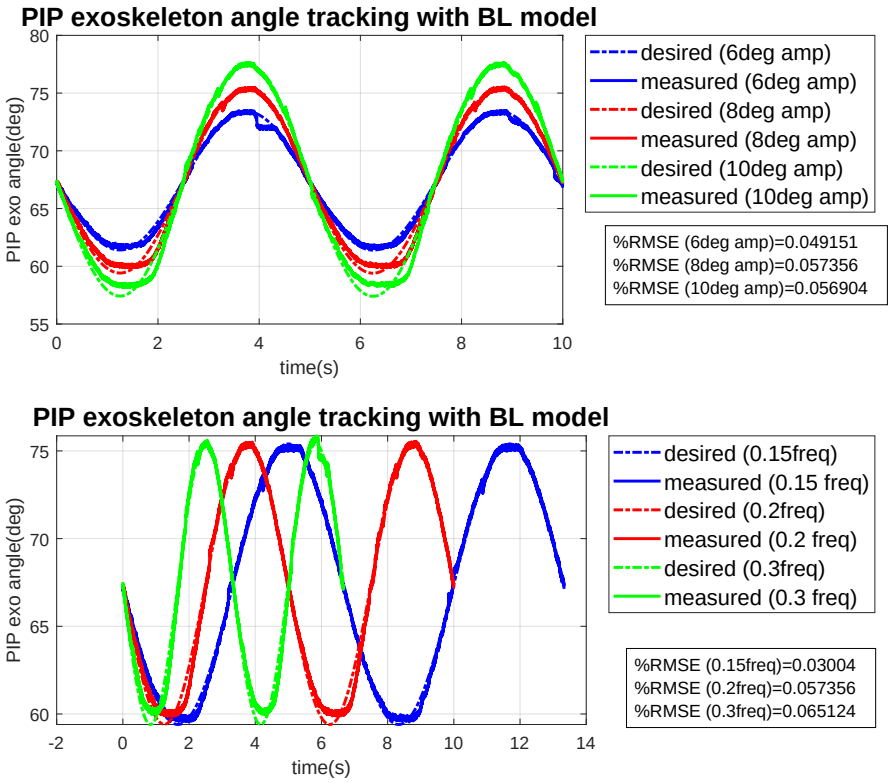

Figure 5.14: Exoskeleton PIP joint angle tracking using the backlash inverse model at three frequencies (0.15 Hz, 0.2 Hz, 0.3 Hz) and three amplitudes (6°, 8°, 10°)

Figure 5.15 shows the exoskeleton angle tracking results for simultaneous tracking of exoskeleton MCP and PIP joints using the backlash inverse model as well the feedback terms.

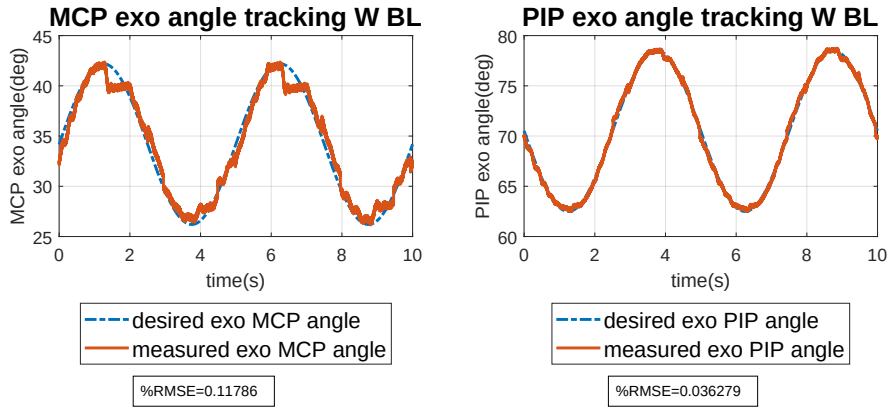

Figure 5.15: Exoskeleton angle tracking utilizing the backlash inverse model. Out-of-phase sinusoidal trajectories are tracked with a frequency of 0.2 Hz and amplitude of 8°.

In Figure 5.16, the exoskeleton angles are shown for a task of tracking exoskeleton PIP joint angle. These data were recorded to investigate effects of movement of one joint on the other.

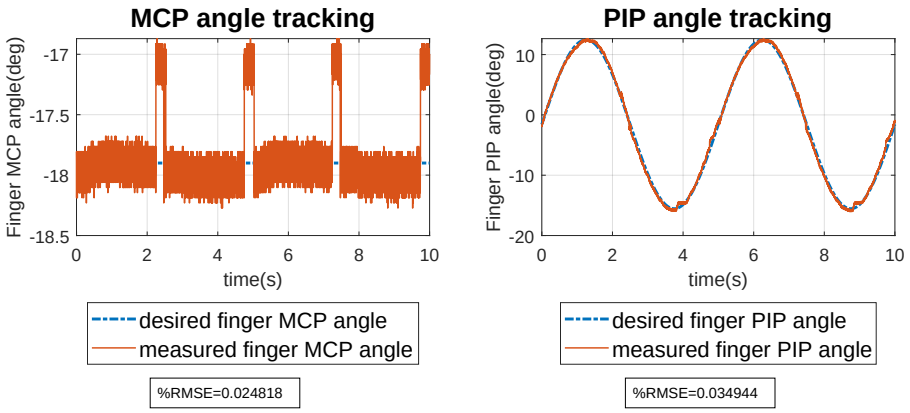

Figure 5.16: Exoskeleton PIP joint angle tracking using the backlash inverse model. Desired exoskeleton PIP joint trajectory is a sinusoidal trajectory with a frequency of 0.2 Hz and amplitude of 8° while MCP joint angle is desired to remain constant.

The finger angle tracking results are shown first for the case of simple feedback based control using finger angle sensor feedback in Figure 5.17. The relationships between the exoskeleton and finger angles are compared for two different movements of finger joints (in-phase and out-of-phase) in Figures 5.18 and 5.19.

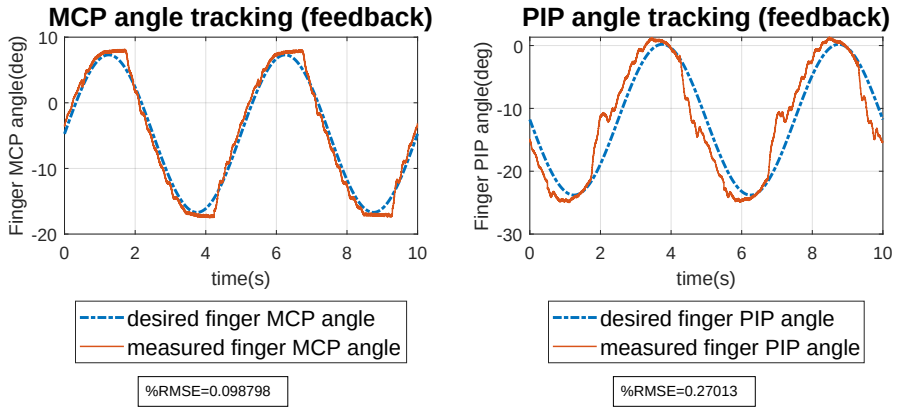

Figure 5.17: Finger angle tracking using feedback from finger angle sensors. Out-of-phase sinusoidal trajectories are tracked with a frequency of 0.2 Hz and amplitude of 12°.

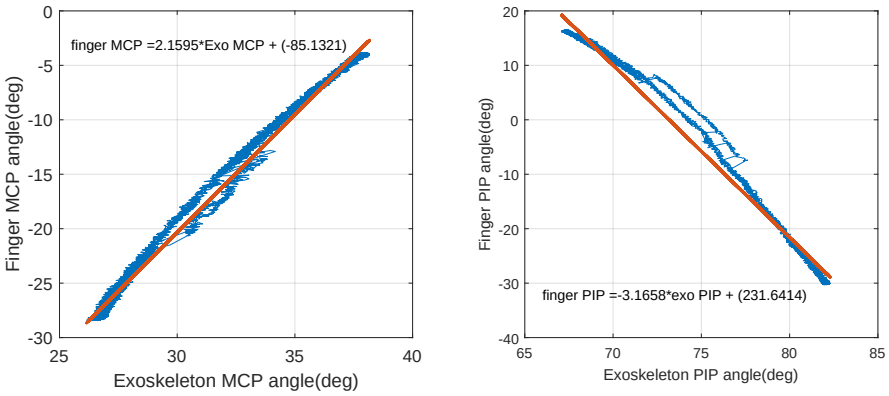

Figure 5.18: Estimating a linear relationship between exoskeleton and finger joint angles in out-of-phase movement of MCP and PIP joint

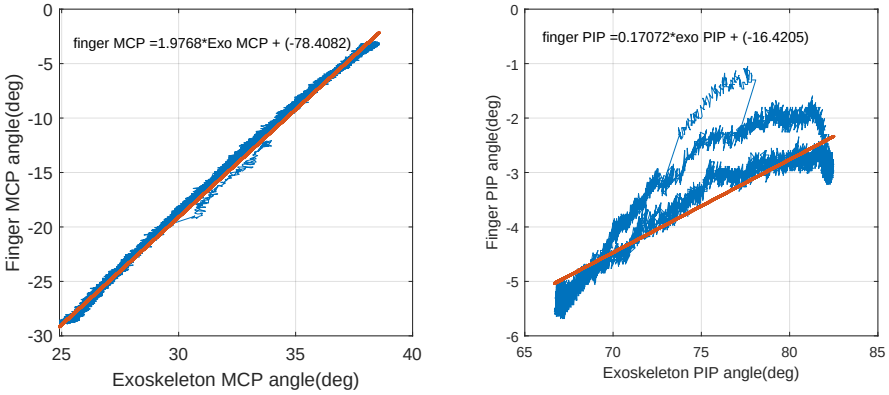

Figure 5.19: Estimating a linear relationship between exoskeleton and finger joint angles in in-phase movement of MCP and PIP joint

Next, the finger angle tracking results are shown in Figure 5.20 using the kinematic-model based control.

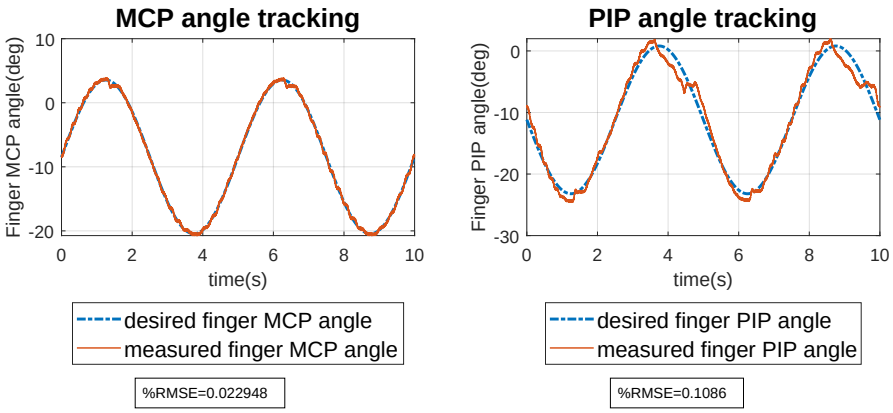

Figure 5.20: Finger angle tracking using the kinematic models. Out-of-phase sinusoidal trajectories are tracked with a frequency of 0.2 Hz and amplitude of 12°.

Finally, the fingertip position tracking results are demonstrated in the following figures. Figures 5.21 shows the fingertip position tracking performance for the task of vertical line tracking in X and Y directions as a function of time. Figure 5.22 shows the X-Y plane projection of desired vertical line and recorded fingertip trajectory. Figure 5.23 shows the X and Y components of the fingertip for a circle trajectory tracking task. And, Figure 5.24 shows the X-Y plane representation.

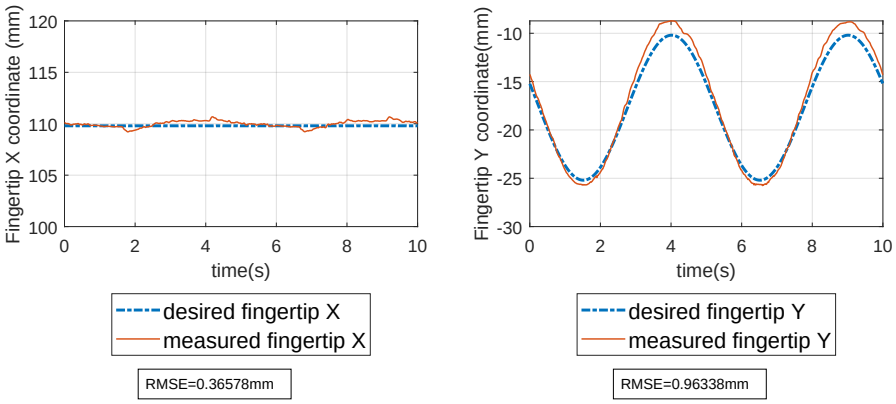

Figure 5.21: Fingertip position tracking performance vs. time for vertical line tracking. Desired trajectory falls in the plane of finger and the length of the line is 1.5 cm.

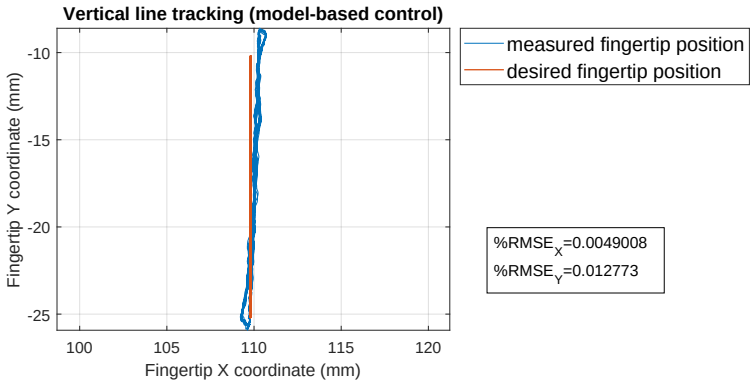

Figure 5.22: X-Y plane demonstration of vertical line tracking performance at the fingertip using model-based control

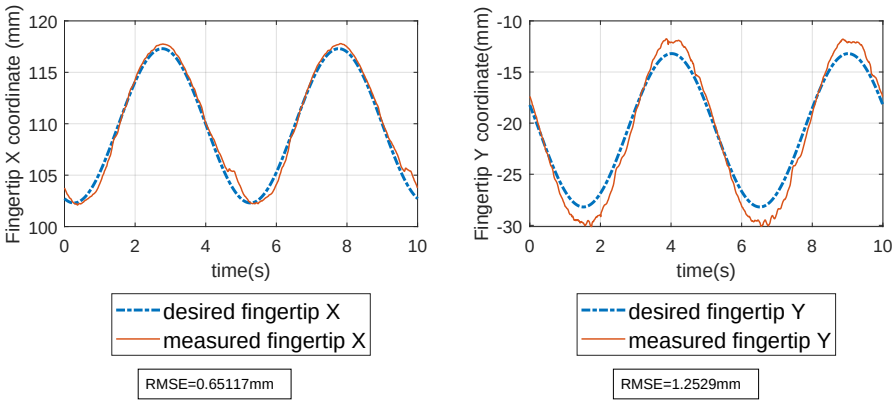

Figure 5.23: Fingertip position tracking performance vs. time for circle trajectory tracking. Desired trajectory falls in the plane of finger and the diameter of the circle is 1.5 cm.

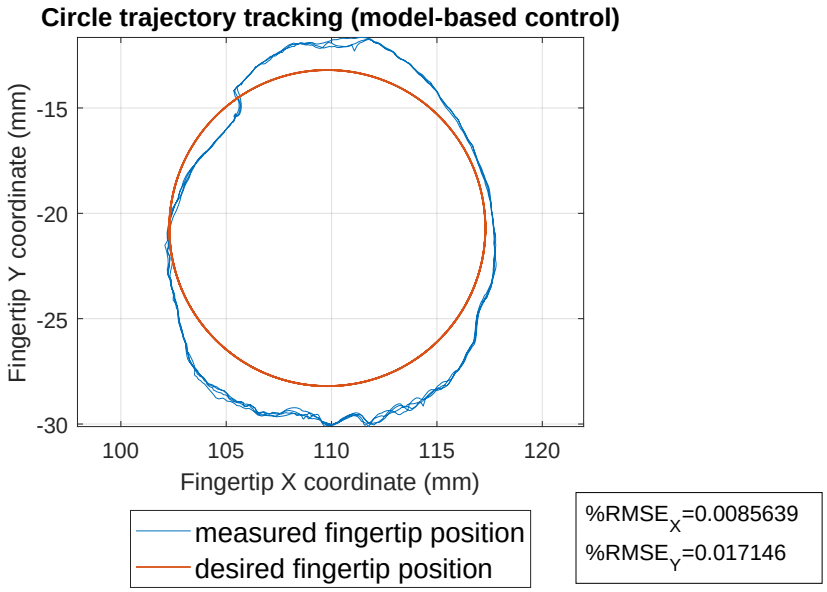

Figure 5.24: X-Y plane demonstration of circle trajectory tracking performance at the fingertip using model-based control

The results of position tracking with human finger are shown in Figure 5.25 for comparison.

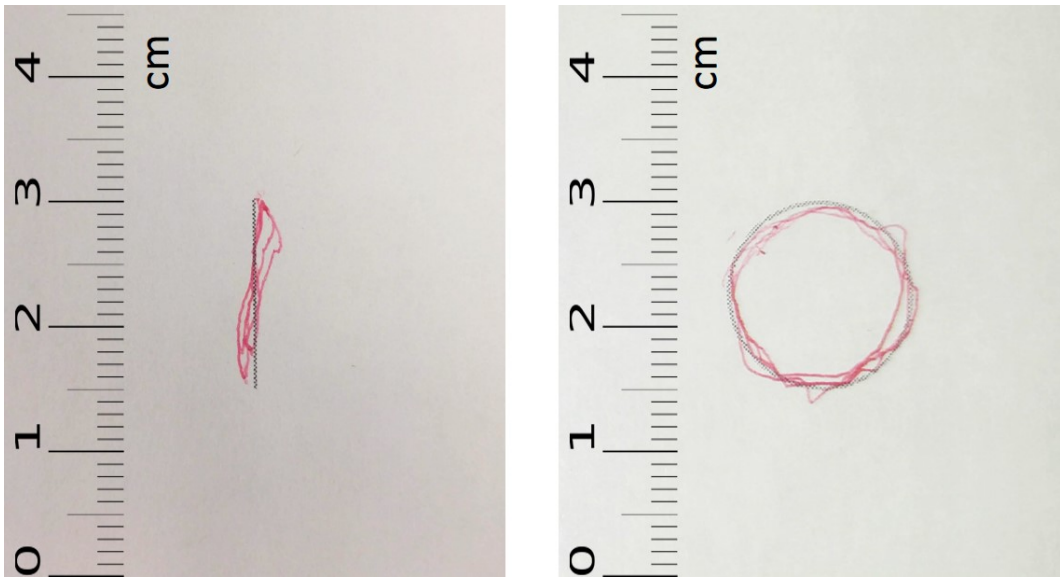

Figure 5.25: Human finger performance in vertical line and circle trajectory tracking tasks. Similar to the assistive exoskeleton case, the movements are performed in the plane of finger, and the length of the line and the diameter of the circle are equal to 1.5 cm.

Performance of the kinematic models related to finger and finger-exo interaction is validated in the following figures. Figure 5.26 shows the estimated values from the finger kinematic model as well as the ground truth values from motion capture recordings for a finger joint angle tracking task. Figure 5.27 demonstrates estimated and measured values for exoskeleton joint angles to evaluate accuracy of kinematic models.

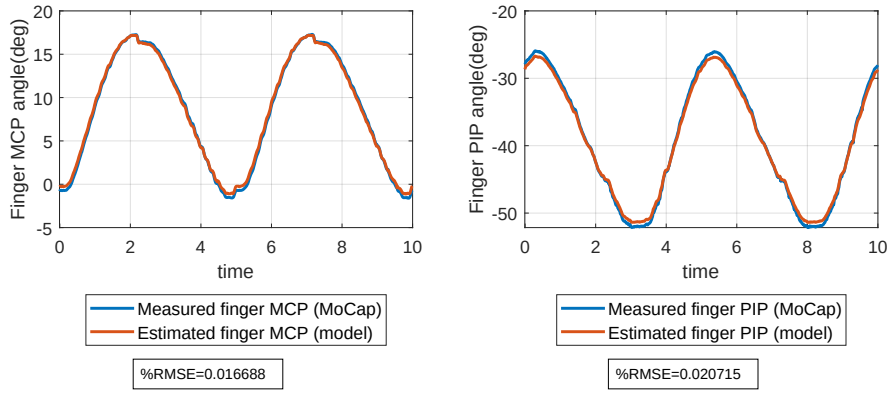

Figure 5.26: Evaluating accuracy of finger kinematic model. Estimated finger angles from the model and measured finger angles from ground truth motion capture are compared.

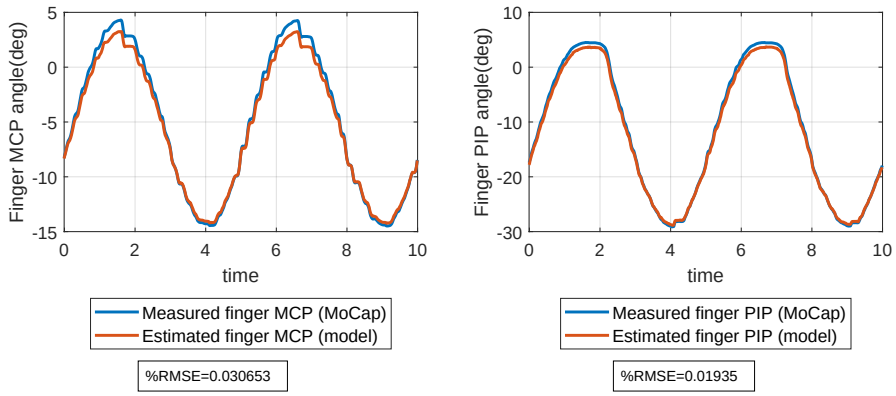

Figure 5.27: Evaluating accuracy of finger-exoskeleton kinematic model. Estimated exoskeleton joint angles from the model and measured exoskeleton joint angles from ground truth motion capture are compared.

Lastly, Figures 5.28 and 5.29 demonstrate the fingertip force tracking results for a vertical force tracking and simultaneous tracking of force in X and Y directions respectively.

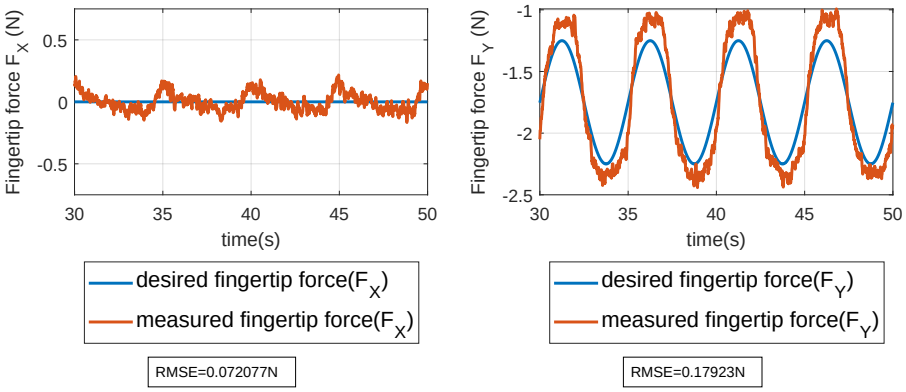

Figure 5.28: Vertical force tracking at the fingertip using the model-based control

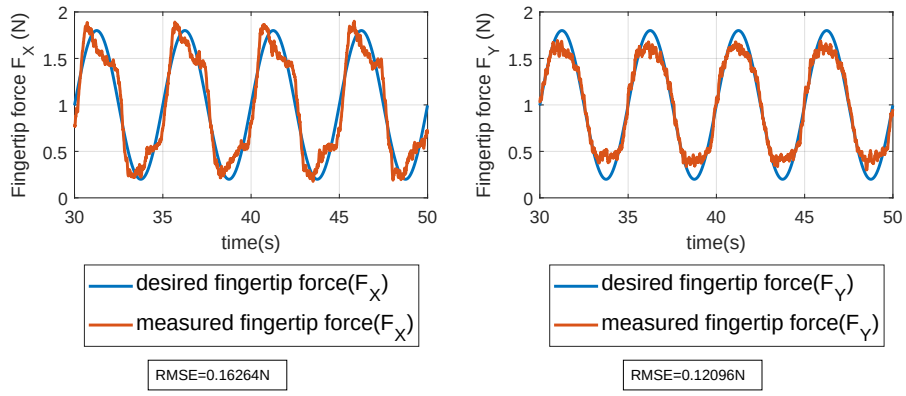

Figure 5.29: Simultaneous tracking of fingertip force in X and Y directions using the model-based control

5.4 Discussion

In this section, we discuss the results from experimental validation with exoskeleton and instrumented finger.

Motor angle tracking accuracy sets the basis for accuracy of other control levels used in this thesis, as any control law used either attempts position tracking by setting motor position to commanded values or performs torque control at the exoskeleton joint through SEA using position control at the motors. According to Figure 5.9, the motor angle tracking percentage RMSE is on the order of 0.01%. Comparing the accuracies in different experiment conditions, we can see that the errors slightly increase as frequency increases. And the RMSE percentage errors slightly decrease as the amplitude increases. The percentage errors are calculated by dividing the RMSE values by the amplitude values.

The second level of position control experiments deal with exoskeleton joint angle tracking, involving Bowden cable transmission system and exoskeleton structure attached to the instrumented finger. Figures 5.10, and 5.11 demonstrate the exoskeleton angle tracking performance assuming perfect transmission system and utilizing feedback from exoskeleton joint angles. The percentage RMS errors are in the range of $0.1\% - 0.22\%$ which are increased by an order of magnitude compared to motor angle tracking errors. The tracking results are generally better for PIP joint of the exoskeleton compared to the MCP joint. This is expected, since the movement of MCP joint results in moving the complete structure of the instrumented finger and the exoskeleton

attached to it, whereas the PIP joint movement only results in moving the distal part of the finger and exoskeleton. Similarly, the errors in this section increase with increasing the frequency of the movement, and percentage errors slightly decrease with increasing amplitudes. Simultaneous tracking of exoskeleton MCP and PIP joints of the exoskeleton is shown in Figure 5.12. The important phenomenon to note in these results is the errors at the peaks of the figures when the angular velocities change direction. The measured values seem to stay unchanged for a short period of time at the peaks and then begin to change, resulting in tracking errors. This error is due to the slack in the transmission system, which appears in most cable driven exoskeleton literature [38, 1] as well as one case with flexible shaft transmission [24], and is addressed in the next approach.

Figures 5.13, and 5.14 demonstrate the exoskeleton angle tracking results implementing the backlash inverse model. We can see that the exoskeleton angle tracking has improved noticeably by taking into account the losses in the transmission system. The percentage RMS errors are within $0.03\% - 0.06\%$, and the angle tracking performance at the peaks is improved using the backlash inverse model that compensates for Bowden cable slack. There are still some inaccuracies at the peaks of the exoskeleton MCP angle tracking figures mainly at the upper peaks. Looking back at the model used to account for Bowden cable backlash (Equation 3.16), the right and left offset values need to be entered manually for each experiment, and the model parameters need to be calibrated before each experiment. The manual values may

contain measurement errors. Moreover, the unmodeled weight of the exoskeleton structure and the finger attached to the exoskeleton results in errors that are more apparent in MCP joint angle tracking results. Figure 5.15 shows the simultaneous angle tracking in exoskeleton MCP and PIP joints. The tracking performance is improved compared to the feedback-based model. However, some inaccuracies are present in the simultaneous tracking case including the over-compensation at the maxima of MCP joint angle trajectory and some other inaccuracies resulting in non-smooth transitions between the peaks in the MCP trajectory. To investigate this more closely, we test the effects of actuating one joint on the other joint's movement. In Figure 5.16, the effects of controlling exoskeleton PIP joint angle is shown on MCP joint movement. Ideally, movement of one joint should not affect the other joint. However, as shown in Figure 3.2, due to the design of the exoskeleton, the two chains of the MCP and PIP joint actuations are connected in point D, which is mounted on a slider. We have assumed once the MCP joint is actuated the location of point D stays unchanged and the PIP chain acts as a pure 4-bar mechanism. However, in reality the dynamics resulting in forces on point D on the slider from the two chains of the exoskeleton result in movement of point D.

The next level of position control is controlling the finger joint angles through the exoskeleton interaction. This level of control includes the structure of the finger, exoskeleton, and the transmission system. Our proposed method as explained in the Methods section is to use the kinematic model of interaction between the exoskeleton and the finger as well as the backlash

inverse model for transmission inaccuracies. However, first the angle tracking results are shown for a case of using simple feedback control using finger angle sensor data bypassing the kinematic and transmission models for comparison. Figure 5.17 demonstrates the finger angle tracking results for a case with out-of-phase movement of MCP and PIP joint angles, implementing the simple feedback control assuming proportional relationship between exoskeleton and finger joint angles. In addition to the effects of Bowden cable backlash in the peaks of MCP angle results, there are errors in PIP angle tracking, increasing the percentage RMS errors to 0.27%. To investigate the relationship between exoskeleton and finger joint angles further, we demonstrate finger angles vs. exoskeleton angles for two cases of out-of-phase and in-phase movements of finger MCP and PIP angles in Figures 5.18 and 5.19. These results imply that the MCP joint angle of the finger may be estimated with a linear relationship with respect to the exoskeleton MCP joint angel within some working range. However, the finger PIP joint angle does not relate to the exoskeleton PIP angle due to the nonlinear nature of the actuation chains. Comparing the two figures, it is apparent that the phase difference between the two joint angle trajectories has an important effect on the dependency of finger PIP joint angle and exoskeleton PIP joint angle. It is important to note that besides the unwanted vibrations in finger angle trajectory tracking caused by using simple feedback control, the finger angle measurements are not accessible in working with human subjects, making this approach impractical in human subject application. On the other hand, Figure 5.20 demonstrates the results

for simultaneous tracking of finger MCP and PIP joint angles according to the control method proposed in this thesis. This control method uses the kinematic models of finger-exoskeleton interaction and the backlash inverse model for transmission. The percentage RMS errors are decreased by more than 50% compared to the simple feedback control, while eliminating the need for direct finger angle measurements.

The final level of position control is fingertip trajectory tracking done in two sample movements, vertical line tracking and circle trajectory tracking. It is important to note that controlling position of the fingertip requires at least the kinematic model of the finger. We attempted controlling the fingertip positions using only the model of the fingers and feedback from finger angles to perform simple feedback control as a comparison similar to finger angle tracking experiments. However, due to the abrupt changes in the control input required the actuators were saturated and it was not possible to perform this task bypassing the kinematic models of interaction between hand and exoskeleton. The model-based control method originally proposed in this thesis uses the kinematic models of the finger, exoskeleton and backlash inverse model to perform fingertip position tracking. Figure 5.21 shows the desired and measured X and Y coordinates of the fingertip for the vertical line tracking task. Figure 5.22 shows the projection in X-Y plane. The percentage RMS errors are less than 0.01% and the RMS error values are less than 1 mm. Similarly, the results for circle trajectory tracking are shown in Figures 5.23 and 5.24. Percentage RMS error values are slightly higher in vertical direction

and are less than 1.3 mm. As mentioned earlier the remaining errors can be due to unmodeled weight, dynamic effects, and compliance of the transmission system. However, we compared the accuracy of the position trajectory tracking results qualitatively with the human finger. Figure 5.25 shows the results for vertical line and circle trajectory tracking performed by a healthy human subject. The trajectories are drawn on a plane parallel to the plane of the finger. Qualitative comparison of the results with trajectory tracking results through exoskeleton control is reassuring that the accuracies are within human finger accuracies that are sufficient for daily activities.

Next, the accuracy of the kinematic models and model parameters for finger structure and exoskeleton-finger interaction are validated in Figures 5.26 and 5.27 for a finger trajectory tracking task. In these two figures, the ground truth motion capture data are compared with estimated angle values from the kinematic models. The two plots closely match and the errors are below 0.04%. It is important to note that the model parameters such as link lengths and relative angle between grounding points of the exoskeleton and finger are acquired from motion capture data as well, and the markers used in the motion capture system have a diameter of 6.4 mm. As a result, some small errors are expected in measurement of model parameters. However, the kinematic models successfully estimate the angles for the required precision used in daily manipulation activities.

Lastly, the results for the fingertip force control in vertical direction and simultaneous control of force in X and Y directions are shown in Figures 5.28,

and 5.29. The errors are below 0.2 N. These results illustrate that using the kinematic models of interaction and the torque control at the exoskeleton joints through SEA, we are able to control the fingertip forces in Cartesian space in X and Y directions.

In summary, the experiment results confirm that fingertip position and force control can be achieved through model-based control of fully actuated finger exoskeleton and transmission system within human finger accuracies. Firstly, using the backlash inverse model for cable driven and flexible shaft actuation allows accurate position control at the exoskeleton joint level. We have also seen the effects of backlash (slack) errors in exoskeleton joint angle control in the literature [38, 1, 24]. In [24], authors have mentioned this to greatly affect the performance of their device. Utilizing the backlash inverse model for joint position control would eliminate this problem, allowing higher accuracies in achieving joint position control. Secondly, implementing the kinematic and kinetic models of interaction between finger and exoskeleton structure allows the control of finger joint positions and torques. Previously, authors in [42] have used the kinematic models of interaction between exoskeleton and finger to control finger joint torques. Our work is the first of its kind to experimentally validate finger joint angle tracking through model-based exoskeleton control. Thirdly, taking into account the finger kinematics and kinetics we were able to track fingertip position as well as direction and magnitude of fingertip force. Unlike a few other studies looking into force control at the fingertip for haptics applications [14, 24], the force control method used in this

thesis does not depend on feedback from force sensors at the fingertip, and can provide directional control of fingertip force. We demonstrated the superior performance of the proposed model-based control compared to feedback-based control in finger joint position tracking and we highlighted the shortcomings of simple feedback based control approaches, which ignore the system kinematics, in fingertip position and force control. The model-based control of the finger exoskeleton system will allow accurate control of position and forces at the fingertip which is a requirement for dexterous manipulation, while also leaving the fingertip space open to interact with objects.

Chapter 6

Conclusion

6.1 Contribution

In this thesis we proposed a modeling-based approach to accurately control fingertip position and forces through assistive hand exoskeletons. We demonstrated that having accurate models of the fingers, the finger-exoskeleton interactions, and the transmission system are necessary to achieve human-like grasping and dexterous manipulation with the help of an exoskeleton. We started with developing the kinematic and kinetic models for finger and thumb modules of a hypothetical exoskeleton design with actuated degrees of freedom in index and middle fingers. We verified in simulation that it is possible to accurately control the fingertip positions and forces at the fingertips. We demonstrated an everyday drawing scenario in which accurate control of the fingertip forces were achieved through the developed models of interaction. Finally, we validated the model-based control by conducting experiments on a simpler testbed with an instrumented finger with two degrees of freedom and the index finger module of Maestro hand exoskeleton. We demonstrated results for successful position tracking at the exoskeleton joints, finger joints and fingertip space. We also compared the proposed modeling and control approach with simpler control methods such as simple feedback-based control from finger joints, demonstrating the effectiveness of the proposed model-based control while eliminating the need for feedback from finger joints. In addition, we successfully performed fingertip force control in Cartesian space in X and Y directions through model-based control. This work is the first of its kind to analyze and control the interactions at the fingertip through model-based con-

trol to enable fine grasping and dexterous manipulation using assistive hand exoskeletons.

Our work has paved the way towards improving assisted grasps and achieving dexterous manipulation with the help of hand exoskeletons. The current research on assistive hand exoskeletons and hand devices has focused on coupling the motion of the fingers and mostly limiting the finger motions to open and close. Using previous strategies fine control of finger motions and fingertip forces was not possible. However, by using a modeling-based approach to control the exoskeletons, humans would be able to fulfill dexterous manipulation tasks. Having accurate models for mapping kinematics and kinetic relationships between exoskeleton, fingers, and fingertips, researchers will be able to implement various control strategies such as stiffness control or impedance control at the fingertips to improve the quality of object manipulation. The modeling approach developed in this work can also be used in different realms of research such as haptics and tele-manipulation. Rendering virtual objects with the help of exoskeletons requires accurate models between the virtual environment and the fingers, as well as finger-exoskeleton interaction models.

6.2 Limitations

The modeling work presented in this thesis has a number of simplifying assumptions. We have neglected the effects of inertia, gravity and dynamics of the hand and the exoskeleton, citing the relatively low inertia of the

two systems as well as low velocities of the finger phalanges in grasping and manipulation tasks. We have achieved accurate control of fingertip forces and positions in this work within human accuracies. However, in this experimental setup we used accurate measurements for model parameters. These measurements are not as easily obtained in human fingers. Therefore, a calibration phase should be used to estimate the model parameters for the fingers in human subject applications. In addition, we have not considered the passive and active properties of the fingers in these models. Although, if the attachments are designed such that the relative movement between fingers and attachment is minimized, using the joint angle sensor data from the exoskeleton and feedback terms in robot control, we would be able to alleviate this problem. The actuators that are used in this robot did not have a homing mechanism. This introduced errors especially in inputting the right and left offsets for the backlash inverse model to compensate for Bowden cable slack in the transmission system. Using an actuation system with a homing mechanism, more accurate results will be achieved in exoskeleton angle tracking through Bowden cable transmission.

6.3 Future Work

In future, we plan to implement similar modeling and control on human thumb and thumb exoskeleton to allow multi-finger dexterous manipulation. In addition, we will extend the model to include object space kinematics and dynamics, as well as stability analysis for object manipulation. This will al-

low the hand and the exoskeleton to perform fine in-hand manipulation with physical objects.

Bibliography

[1] Priyanshu Agarwal, Jonas Fox, Youngmok Yun, Marcia K. O'Malley, and Ashish D. Deshpande. An index finger exoskeleton with series elastic actuation for rehabilitation: Design, control and performance characterization. *The International Journal of Robotics Research*, 34(14):1747–1772, 2015.

[2] Priyanshu Agarwal, Youngmok Yun, Jonas Fox, Kaci Madden, and Ashish D. Deshpande. Design, control, and testing of a thumb exoskeleton with series elastic actuation. *The International Journal of Robotics Research*, 36(3):355–375, 2017.

[3] Priyanshu Agarwal, Youngmok Yun, Jonas Fox, Kaci Madden, and Ashish D. Deshpande. Design, control, and testing of a thumb exoskeleton with series elastic actuation. *The International Journal of Robotics Research*, 36(3):355–375, 2017.

[4] Patrick M Aubin, Hani Sallum, Conor Walsh, Leia Stirling, and Annette Correia. A pediatric robotic thumb exoskeleton for at-home rehabilitation: the isolated orthosis for thumb actuation (iota). In *Rehabilitation Robotics (ICORR), 2013 IEEE International Conference on*, pages 1–6. IEEE, 2013.

[5] Nisim Benjuya and Steven B Kenney. Myoelectric hand orthosis. *JPO: Journal of Prosthetics and Orthotics*, 2(2):149–154, 1990.

[6] Marco Cempini, Mario Cortese, and Nicola Vitiello. A powered finger–thumb wearable hand exoskeleton with self-aligning joint axes. *IEEE/ASME Transactions on mechatronics*, 20(2):705–716, 2015.

[7] Marco Cempini, Alberto Marzegan, Marco Rabuffetti, Mario Cortese, and Nicola Vitiello. Analysis of relative displacement between the HX wearable robotic exoskeleton and the user's hand. 2014.

[8] Fai Chen Chen, Silvia Appendino, Alessandro Battezzato, Alain Favetto, Mehdi Mousavi, and Francesco Pescarmona. Constraint study for a hand exoskeleton: human hand kinematics and dynamics. *Journal of Robotics*, 2013, 2013.

[9] Salvador Cobos, Manuel Ferre, MA Sanchez Uran, Javier Ortego, and Cesar Pena. Efficient human hand kinematics for manipulation tasks. In *Intelligent Robots and Systems, 2008. IROS 2008. IEEE/RSJ International Conference on*, pages 2246–2251. IEEE, 2008.

[10] R Conti, E Meli, and A Ridolfi. A novel kinematic architecture for portable hand exoskeletons. *Mechatronics*, 35:192–207, 2016.

[11] John J Craig. Introduction to robotics: Manipulation and control, 1986.

[12] Ashish D. Deshpande, Zhe Xu, Michael J. vande Weghe, Benjamin H Brown, Jonathan Ko, Lillian Y Chang, David D Wilkinson, Sean M Bidic,

and Yoky Matsuoka. Mechanisms of the anatomically correct testbed hand. *IEEE/ASME Transactions on Mechatronics*, 18(1):238–250, 2013.

[13] Matthew DiCicco, Lenny Lucas, and Yoky Matsuoka. Comparison of control strategies for an emg controlled orthotic exoskeleton for the hand. In *Robotics and Automation, 2004. Proceedings. ICRA'04. 2004 IEEE International Conference on*, volume 2, pages 1622–1627. ieee, 2004.

[14] Marco Fontana, Salsedo Fabio, Simone Marcheschi, and Massimo Bergamasco. Haptic hand exoskeleton for precision grasp simulation. *Journal of Mechanisms and Robotics*, 5(4):041014, 2013.

[15] Massimiliano Gabardi, Massimiliano Solazzi, Daniele Leonardis, and Antonio Frisoli. Design and evaluation of a novel 5 dof underactuated thumb-exoskeleton. *IEEE Robotics and Automation Letters*, 3(3):2322–2329, 2018.

[16] Vikash Gupta. Kinematic analysis of a thumb-exoskeleton system for post-stroke rehabilitation. Master's thesis, 2010.

[17] Yasuhisa Hasegawa, Yasuyuki Mikami, Kosuke Watanabe, and Yoshiyuki Sankai. Five-fingered assistive hand with mechanical compliance of human finger. In *Robotics and Automation, 2008. ICRA 2008. IEEE International Conference on*, pages 718–724. IEEE, 2008.

[18] Neville Hogan. Impedance control: An approach to manipulation. In *American Control Conference, 1984*, pages 304–313. IEEE, 1984.

[19] Hyunki In, Brian Byunghyun Kang, MinKi Sin, and Kyu-Jin Cho. Exoglove: A wearable robot for the hand with a soft tendon routing system. *IEEE Robotics & Automation Magazine*, 22(1):97–105, 2015.

[20] Christopher L Jones, Furui Wang, Robert Morrison, Nilanjan Sarkar, and Derek G Kamper. Design and development of the cable actuated finger exoskeleton for hand rehabilitation following stroke. *IEEE/ASME Transactions on Mechatronics*, 19(1):131–140, 2014.

[21] Yasuhisa Kamikawa and Takashi Maeno. Underactuated five-finger prosthetic hand inspired by grasping force distribution of humans. In *Intelligent Robots and Systems, 2008 IEEE/RSJ International Conference on (IROS)*, pages 717–722. IEEE, 2008.

[22] Tatsuya Koyama, Ikuo Yamano, Kenjiro Takemura, and Takashi Maeno. Multi-fingered exoskeleton haptic device using passive force feedback for dexterous teleoperation. In *IEEE/RSJ International Conference on Intelligent Robots and Systems*, volume 3, pages 2905–2910. IEEE, 2002.

[23] J. Li, R. Zheng, Y. Zhang, and J. Yao. iHandRehab: An interactive hand exoskeleton for active and passive rehabilitation. In *2011 IEEE International Conference on Rehabilitation Robotics*, pages 1–6, June 2011.

[24] Jiting Li, Shuang Wang, Ju Wang, Ruoyin Zheng, Yuru Zhang, and Zhongyuan Chen. Development of a hand exoskeleton system for index finger rehabilitation. *Chinese journal of mechanical engineering*, 25(2):223–233, 2012.

[25] Nina Lightdale-Miric, Nicole M Mueske, Sudarshan Dayanidhi, Jennifer Loiselle, Jamie Berggren, Emily L Lawrence, Milan Stevanovic, Francisco J Valero-Cuevas, and Tishya AL Wren. Quantitative assessment of dynamic control of fingertip forces after pollicization. *Gait & posture*, 41(1):1–6, 2015.

[26] John Lin, Ying Wu, and Thomas S Huang. Modeling the constraints of human hand motion. In *Human Motion, 2000. Proceedings. Workshop on*, pages 121–126. IEEE, 2000.

[27] Lenny Lucas, Matthew DiCicco, and Yoky Matsuoka. An EMG-controlled hand exoskeleton for natural pinching. *Journal of Robotics and Mechatronics*, 16:482–488, 2004.

[28] Natsuki Miyata, Makiko Kouchi, Tsuneya Kurihara, and Masaaki Mochimaru. Modeling of human hand link structure from optical motion capture data. In *2004 IEEE/RSJ International Conference on Intelligent Robots and Systems (IROS)(IEEE Cat. No. 04CH37566)*, volume 3, pages 2129–2135. IEEE, 2004.

[29] Taylor D Niehues. *Achieving human-like dexterity in robotic hands: inspiration from human hand biomechanics and neuromuscular control*. PhD thesis, 2017.

[30] Robert L Norton and Sid Shih-Liang Wang. *Design of machinery: an introduction to the synthesis and analysis of mechanisms and machines*. McGraw-Hill Higher Education, 2004.

[31] Panagiotis Polygerinos, Zheng Wang, Kevin C Galloway, Robert J Wood, and Conor J Walsh. Soft robotic glove for combined assistance and at-home rehabilitation. *Robotics and Autonomous Systems*, 73:135–143, 2015.

[32] Shu-Wei Pu, Sung-Yu Tsai, and Jen-Yuan Chang. Design and development of the wearable hand exoskeleton system for rehabilitation of hand impaired patients. In *Automation Science and Engineering (CASE), 2014 IEEE International Conference on*, pages 996–1001. IEEE, 2014.

[33] Yupeng Ren, Hyung-Soon Park, and Li-Qun Zhang. Developing a whole-arm exoskeleton robot with hand opening and closing mechanism for upper limb stroke rehabilitation. In *Rehabilitation Robotics, 2009. ICORR 2009. IEEE International Conference on*, pages 761–765. IEEE, 2009.

[34] Veronica J Santos and Francisco J Valero-Cuevas. Reported anatomical variability naturally leads to multimodal distributions of denavit-hartenberg parameters for the human thumb. *IEEE Transactions on Biomedical Engineering*, 53(2):155–163, 2006.

[35] Hossein Taheri, Justin B Rowe, David Gardner, Vicki Chan, Kyle Gray, Curtis Bower, David J Reinkensmeyer, and Eric T Wolbrecht. Design and preliminary evaluation of the finger rehabilitation robot: controlling challenge and quantifying finger individuation during musical computer game play. *Journal of neuroengineering and rehabilitation*, 11(1):10, 2014.

[36] Satoshi Ueki, Haruhisa Kawasaki, Satoshi Ito, Yutaka Nishimoto, Motoyuki Abe, Takaaki Aoki, Yasuhiko Ishigure, Takeo Ojika, and Tetsuya Mouri. Development of a hand-assist robot with multi-degrees-of-freedom for rehabilitation therapy. *IEEE/ASME Transactions on mechatronics*, 17(1):136–146, 2012.

[37] Furui Wang, Christopher L Jones, Milind Shastri, Kai Qian, Derek G Kamper, and Nilanjan Sarkar. Design and evaluation of an actuated exoskeleton for examining motor control in stroke thumb. *Advanced Robotics*, 30(3):165–177, 2016.

[38] Furui Wang, Milind Shastri, Christopher L Jones, Vikash Gupta, Christian Osswald, Xuan Kang, Derek G Kamper, and Nilanjan Sarkar. Design and control of an actuated thumb exoskeleton for hand rehabilitation following stroke. In *Robotics and Automation (ICRA), 2011 IEEE International Conference on*, pages 3688–3693. IEEE, 2011.

[39] Andreas Wege and Günter Hommel. Development and control of a hand exoskeleton for rehabilitation of hand injuries. In *2005 IEEE/RSJ International Conference on Intelligent Robots and Systems*, pages 3046–3051. IEEE, 2005.

[40] Yoshihiro Yasumuro, Qian Chen, and Kunihiro Chihara. Three-dimensional modeling of the human hand with motion constraints1. *Image and Vision Computing*, 17(2):149–156, 1999.

[41] Youngmok Yun, Priyanshu Agarwal, and Ashish D. Deshpande. Accurate, robust, and real-time pose estimation of finger. *Journal of Dynamic Systems, Measurement, and Control*, 137(3-35):034505, 2015.

[42] Youngmok Yun, Priyanshu Agarwal, Jonas Fox, Kaci E Madden, and Ashish D. Deshpande. Accurate torque control of finger joints with ut hand exoskeleton through bowden cable sea. In *Intelligent Robots and Systems (IROS), 2016 IEEE/RSJ International Conference on*, pages 390–397. IEEE, 2016.

[43] Youngmok Yun, Sarah Dancausse, Paria Esmatloo, Alfredo Serrato, Curtis A Merring, Priyanshu Agarwal, and Ashish D. Deshpande. Maestro: An emg-driven assistive hand exoskeleton for spinal cord injury patients. In *Robotics and Automation (ICRA), 2017 IEEE International Conference on*, pages 2904–2910. IEEE, 2017.

[44] Youngmok Yun, Paria Esmatloo, Alfredo Serrato, Curtis A Merring, and Ashish D. Deshpande. Methodologies for determining minimal grasping requirements and sensor locations for sEMG-based assistive hand orthosis for SCI patients. In *Rehabilitation Robotics (ICORR), 2017 International Conference on*, pages 746–752. IEEE, 2017.

[45] Ruoyin Zheng and Jiting Li. Kinematics and workspace analysis of an exoskeleton for thumb and index finger rehabilitation. In *Robotics and Biomimetics (ROBIO), 2010 IEEE International Conference on*, pages 80–84. IEEE, 2010.

[46] MA Zhou and Pinhas Ben-Tzvi. Rml glovean exoskeleton glove mechanism with haptics feedback. *IEEE/ASME Transactions on Mechatronics*, 20(2):641–652, 2015.